Material Recovery and Evaluation of Recycled Disassembled Automotive Plastic Components: Enabling the Automotive Circular Economy

A Thesis Presented for the

Master of Science

Degree

The University of Tennessee, Knoxville

Neeki Meshkat

August 2025

Copyright © 2025 by Neeki Meshkat

All rights reserved.

ACKNOWLEDGEMENTS

I would like to express my sincere appreciation to my advisor, Dr. Uday Vaidya, for providing me with the opportunity to pursue a master's degree under his guidance. I am especially grateful to Dr. Matthew Korey, his support, encouragement, and mentorship throughout this journey has been invaluable, helping me grow both personally and professionally. I am forever thankful to have had him as my mentor. A special thanks to Dr. Amber Hubbard for teaching me how to interpret data from the ground up, reviewing manuscript drafts and presentation slides, and offering insightful suggestions along the way. I am very grateful for your guidance. I would also like to thank Dr. Krishnan Veluswamy for serving on my committee and for offering thoughtful feedback and directions for my work.

I would also like to acknowledge and thank all the members of the Sustainable Manufacturing Technologies (SMT) group at the Manufacturing Demonstration Facility (MDF) at Oak Ridge National Laboratory (ORNL), especially, Dr. Soydan Ozcan, Dr. Katie Copenhaver, Dr. Caitlyn Clarkson and Dr. Sanjita Wasti for their support. I would like to acknowledge and thank Tristan McGill and Deserae Goldsby for their efforts in shredding and collecting the ELV plastic components used in this work. I am also thankful to Pete Glenister at LyondellBasell for supplying the control materials for analysis. To my friends and colleagues at MDF, Komal Kooduvalli, Kathryn Slavny, Ashish Anilal, and Roo Walker, thank you for your support, motivation, and camaraderie throughout this process. I'd like to thank Ryan Ogle for taking the time to train me on the injection molder at MDF, help troubleshoot machine issues and assist with the many

mold changes throughout the process. I would also like to extend my thanks to Dr. Jacob Kinnun for his assistance and guidance with machine training at the Institute for Advanced Materials & Manufacturing (IAMM). I also extend my gratitude to the former and current staff, graduate students, and undergraduate students at the Fibers and Composites Manufacturing Facility (FCMF).

I am forever grateful to the most important people in my life, my mom Leila Meshkat, my dad Masoud Meshkat, my brother Ali Meshkat, and my sister Bahar Meshkat, for their unwavering love and support.

I would like to thank the American Chemistry Council and Oak Ridge National Laboratory for their collaboration under the 2021 Memorandum of Understanding that enabled this work. I am also grateful to the U.S. Department of Energy for funding this research, with Oak Ridge National Laboratory operated by UT-Battelle, LLC.

ABSTRACT

As the automotive industry increasingly relies on plastic components to meet fuel efficiency and emissions targets, the challenge of managing end-of-life vehicle (ELV) plastics continues to grow. Currently, more than 80% of ELV plastics in the U.S. are landfilled due to limited economic incentives and technical barriers to recycling. This study examines a mechanical recycling pathway for thermoplastic components disassembled from End-of-Life Vehicles (ELVs) and assesses their usability for reintegration into new vehicle parts. Four representative materials were chosen based on material labels embedded in recovered parts and aligned with their virgin industrial equivalents: polypropylene (PP), 10% talc-filled PP (PP-T10), 20% talc-filled PP (PP-T20), and a 20% glass/mineral-filled polyamide (PA6+GF7+MF13). The materials underwent shredding, drying, and injection molding before being characterized by particle size analysis, density measurement, thermal analysis (TGA, DSC), mechanical testing, and heat deflection temperature (HDT) evaluation. Results indicate that while minor changes in density and crystallinity occurred, mechanical properties such as Young's Modulus and ultimate tensile strength (UTS) remained largely within functional ranges for automotive applications, particularly for filled PP and PA6 samples. These findings suggest that mechanically recycled, disassembled ELV plastics can retain sufficient structural performance to support circularity efforts in the automotive sector.

TABLE OF CONTENTS

Chapter One Introduction 1

The Rise of Plastics in the Automotive Industry 1

The Role of Plastics in Vehicle Safety 1

Material Advantages and Cost Considerations 3

End-of-Life Pathways for Automotive Plastics 4

End-of-Life Vehicle (ELV) Management and Disposal Costs 7

Policy and Regulatory Landscape 8

Sequence of Document 9

Chapter Two Literature Review 10

Life Cyle Assessment Frameworks 14

Barrier to ELV Plastic Recovery 15

Automotive Industry Attempts to Recycle Plastics 16

Academic Research Models 18

Objectives of the Present Study 19

Chapter Three methods and Materials 20

Materials 20

ELV Disassembly 20

Sample Preparation 21

Characterization 29

Particle Size Analysis 29

Density 30

FTIR 30
TGA 31
DSC 31
HDT 32
Mechanical Testing 32
Chapter Four Results and Discussion 34
Particle Size Analysis & Sample Density 34
Fourier Transform Infrared Spectroscopy (FTIR) 36
Thermal Behavior: Differential Scanning Calorimetry (DSC) 40
Thermal Degradation: Thermogravimetric Analysis (TGA) 43
Combined DSC–TGA Thermal and Crystallinity Trends 46
Mechanical Performance 53
Chapter Five Conclusions and Recommendations 60
Appendix 72
VITA 82

LIST OF TABLES

Table 3.1 - Mass flow data for shredded ELV samples. For each part, the table includes the original feedstock weight, total granulate collected, the portion recovered by vacuum, and estimated material loss during shredding. A dash (–) indicates no record was taken. 28

Table 4.1 - Residual mass at 600 °C (%) and temperature (°C) at 2% weight loss measured by TGA. Values are grouped by stage: Virgin Pellet, End-of-Life (EOL) 45

Table 5.1 - DSC results comparing virgin pellets with end-of-life (EOL) materials. Values reflect thermal properties during both the first and second heating cycles. . 72

Table 5.2 - DSC results comparing injection molded virgin pellets and injection molded recycled granules. Values reflect thermal properties during both the first and second heating cycles. 75

Table 5.3 - Residual mass at 600 °C (%) and temperature (°C) at 2% weight loss measured by TGA. Values are grouped by stage: Injection Molded Virgin Pellet, and Injection Molded Recycled Granule. 77

LIST OF FIGURES

Figure 1.1 - The amount of plastic in vehicles in the U.S since 1960 [8]..... 2

Figure 1.2 - Composition Of Plastics Used In Automobiles By Type. Adapted from *EuRIC Call for Recycled Plastic Contentin Cars* 2020..... 3

Figure 1.3 - Overview of ELV Recycling Pathway Based on EU Regulatory Directive. .. 6

Figure 2.1 - Overview of Plastic Recycling Technologies and Their Suitability for ELV Waste Streams adapted from Jiang. X et al. 13

Figure 3.1 Photographic overview of disassembled end-of-life vehicle (ELV) components selected for mechanical recycling. Four thermoplastic parts were manually recovered from a vehicle and identified by their embedded material markings: (a) engine cover (PA6+GF7+MF13), (b) deck trim cover (PP-T10), (c) front bumper fascia (PP), and (d) trunk interior panel (PP-T20).The central illustration maps the approximate location of each part on the vehicle. 22

Figure 3.2 Close-up image of embedded part labeling on the disassembled engine cover. The molding indicates the material (PA6+GF7+MF13), the manufacturer Kia, and the original part number, allowing identification and tracking of the base polymer and filler content. 23

Figure 3.3 - Visualization of the process pathway for mechanical recycling of EOL vehicle plastics. 24

Figure 3.4 Internal views of the GP20 plastic recycling system. (a) Shredder chamber showing the interlocking combs and rotating blades used to break down large

polymer parts. (b) Granulator unit with a rotating cutting blade and cylindrical mesh screen used to achieve consistent particle sizing below 4 mm. 25

Figure 3.5 - Normalized material recovery breakdown by polymer and ELV component. Bars represent the mass distribution of each sample as a percentage of its starting feedstock. Recovered material is divided into portions captured directly in the hopper and manually recovered by vacuum, with the remaining mass attributed to shredding loss. Components include a bumper (PP), deck trim (PP-T10), trunk panel (PP-T20), and engine cover (PA6+GF7+MF13). 27

Figure 3.6 ASTM Type V dog bone sample mounted for tensile testing in an Instron universal testing machine. 33

Figure 4.1- a) Particle Size Analysis of both granulated and virgin pellet samples. b) Average density of injected molded parts made from both virgin pellets and recycled granules. 35

Figure 4.2 - FTIR spectra of injection molded virgin PP pellets and injection molded recycled PP granules 38

Figure 4.3 - FTIR spectra of injection molded virgin PP-T10 pellets and injection molded recycled PP-T10 granules. 38

Figure 4.4 - FTIR spectra of injection molded virgin PP-T20 pellets and injection molded recycled PP-T20 granules 39

Figure 4.5 - FTIR spectra of injection molded virgin PA6+GF7+MF13 pellets and injection molded recycled PA6+GF7+MF13 granules. 39

Figure 4.6 - DSC thermograms comparing virgin pellets and end-of-life (EOL) samples for all four material formulations from first heat cycle 41
Figure 4.7 - DSC thermograms comparing virgin pellets and end-of-life (EOL) samples for all four material formulations from second heat cycle..... 42
Figure 4.8 - Thermogravimetric analysis (TGA) curves showing mass loss profiles for virgin and recycled samples of all four material formulations. Virgin samples are shown as dashed lines; EOL samples as solid lines..... 44
Figure 4.9 - Melting temperature, crystallinity, and residual mass at 600 °C for PP samples across all processing stages, based on DSC and TGA data from the first heating cycle. 47
Figure 4.10 - Melting temperature, crystallinity, and residual mass at 600 °C for PP-T10 samples across all processing stages, based on first heat thermal analysis. 49
Figure 4.11 - Melting temperature, crystallinity, and residual mass at 600 °C for PP-T20 samples across all processing stages, derived from first heat DSC and TGA measurements..... 51
Figure 4.12 - Melting temperature, crystallinity, and residual mass at 600 °C for PA6+GF7+MF13 samples across all processing stages, as measured in the first heating cycle of DSC and TGA. 52
Figure 4.13 - Young's modulus and ultimate tensile strength of PP injection molded parts made from virgin pellets and recycled granules. 54
Figure 4.14 - Young's modulus and ultimate tensile strength of PP-T10 injection molded parts made from virgin pellets and recycled granules. 55

Figure 4.15 - Young's modulus and ultimate tensile strength of PP-T20 injection molded parts made from virgin pellets and recycled granules. 57
Figure 4.16 - Young's modulus and ultimate tensile strength of PA6-GF7-MF13 injection molded parts made from virgin pellets and recycled granules. 57
Figure 4.17 - Heat deflection temperature (°C) results from injected molded parts made from both virgin pellets and recycled granulates. 58
Figure 5.1 - DSC thermograms comparing injection molded virgin pellets and injection molded recycled granules samples for all four material formulations for first heat. 73
Figure 5.2 - DSC thermograms comparing injection molded virgin pellets and injection molded recycled granules samples for all four material formulations for second heat. 74
Figure 5.3 - Thermogravimetric analysis (TGA) curves showing mass loss profiles for injection molded virgin and recycled samples across all four material formulations. Virgin samples are shown as solid lines, recycled samples as dashed lines. 76
Figure 5.4 - Melting temperature and crystallinity for PP samples across all processing stages, based on second heat thermal analysis. 78
Figure 5.5 - Melting temperature and crystallinity for PP-T10 samples across all processing stages, based on second heat thermal analysis 79
Figure 5.6 - Melting temperature and crystallinity for PP-T20 samples across all processing stages, based on second heat thermal analysis 80
Figure 5.7 - Melting temperature and crystallinity for PA6+GF7+MF13 samples across all .processing stages, based on second heat thermal analysis 81

CHAPTER ONE

INTRODUCTION

The Rise of Plastics in the Automotive Industry

The automotive industry is one of the largest global markets, with annual vehicle production reaching 94 million units in 2023 and growing at an average annual rate of 3.8% in the U.S., as seen in **Figure 1.1** [1-3]. Vehicles are complex, multi-material assemblies incorporating high-value components, with an average market value of approximately 50,000 USD [4]. A vehicle's core structural framework is typically made from high-strength steel or aluminum. The bulk of the rest of the materials in a vehicle are a mixture of metals, glass, rubber, fiber-reinforced/advanced composites, and plastics. In the search for greater fuel efficiency and lower emissions, the automotive industry has learned that replacing heavier materials like metal with plastics helps reduce vehicle weight [2, 5]. As such, between 2012 and 2021, the average amount of plastics in automobiles increased by 16%, reaching up to 411 pounds per vehicle [6]. This increase in plastic usage at least partially increased fuel efficiency by 6–8% and reduced CO_2 emissions by approximately 7.6 grams per kilometer (g/km) driven [2].

The Role of Plastics in Vehicle Safety

The transition to plastics and composites has also significantly improved vehicle efficiency. Certain materials can absorb more energy during a crash than metals, translating to better absorb impact energy and lower occupant risk. Studies have shown that carbon-fiber-reinforced polymers (CFRPs), for instance, demonstrate higher specific energy absorption (SEA) and more stable force-displacement behavior under impact

loading compared to traditional aluminum alloys [7]. These properties make composites highly valuable in enhancing crash protection without adding significant weight. As vehicle crash standards become more severe, the automotive industry has increasingly relied on plastic-based materials to meet both safety and performance targets. Beyond their critical role in crash performance, plastics also offer notable manufacturing and cost advantages that have further fueled their integration in automotive design. However, the same characteristics that make plastics appealing during production and use can become troublesome at end-of-life, where recovery remains technologically and economically challenging.

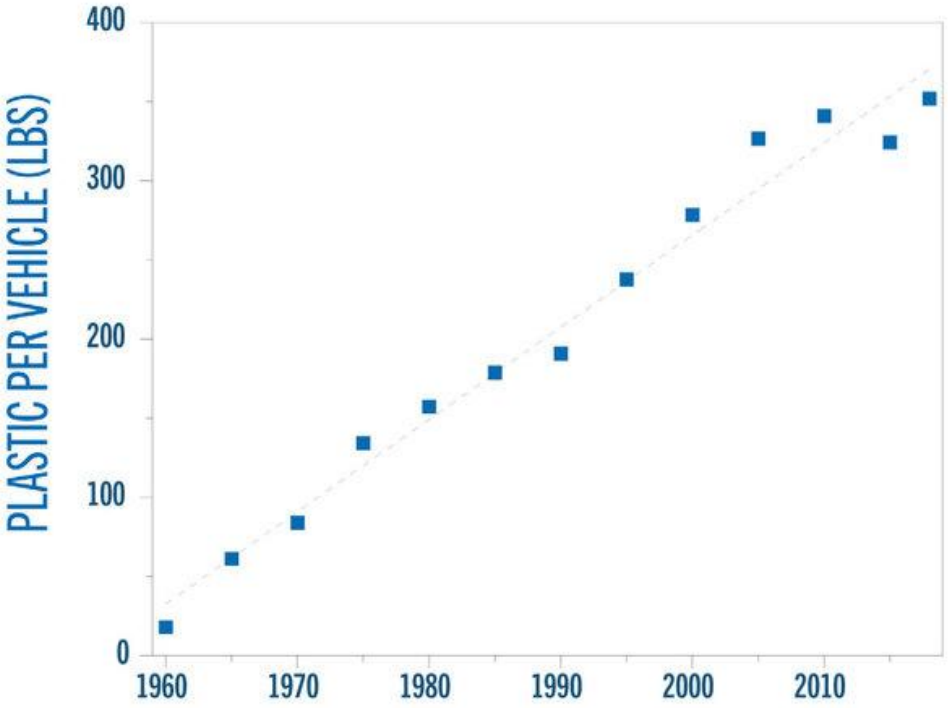


Figure 1.1 - The amount of plastic in vehicles in the U.S since 1960 [8]

Material Advantages and Cost Considerations

Modern automobiles consist of more than 50% plastic by volume, but due to their low density, they contribute to less than 10% of the vehicle's weight [8]. Currently, PP constitutes 32% of the total plastic used in vehicles, followed by polyurethane (PU) at 17%, polyvinyl chloride (PVC) at 16%, and polyamide (PA) at 12%. Collectively, these materials make up 78% of all automotive plastics as seen in **Figure 1.2** [9].

Lower-cost materials like PP, PU, PVC, and other plastics are commonly used in bumpers, insulation, seating, and interior components. PA, however, comes at a higher cost (2.82 USD/kg) compared to other commonly used plastics PP is approximately (1.20 USD/kg) [10]. For these reasons, it has found applications in higher-performance, higher value components in the vehicle, such as intake manifolds, engine covers, radiator end tanks, and structural brackets.

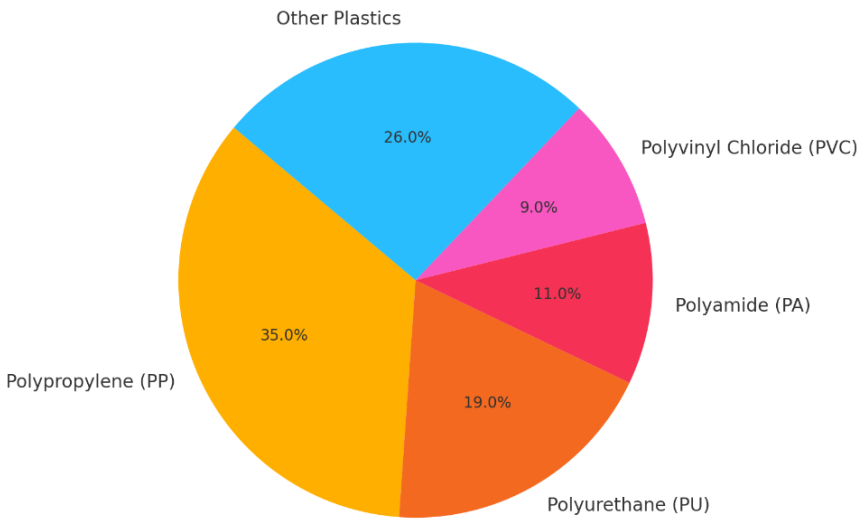


Figure 1.2 - Composition Of Plastics Used In Automobiles By Type. Adapted from *EuRIC Call for Recycled Plastic Contentin Cars* 2020

Plastics are more manufacturable and enable more complex multi-material assemblies than metals. They can be processed using various manufacturing techniques, including injection molding, thermoforming, blow molding, and increasingly additive manufacturing. These processes allow for lightweight designs, rapid prototyping, high-rate compression molding, and integrated part consolidation, offering both performance and cost advantages in vehicle production [11]. While it is undeniable that plastics offer tremendous benefits during the vehicle's service life, unlike metals, their disposal presents a growing challenge at end-of-life.

End-of-Life Pathways for Automotive Plastics

Each year, between 12 and 15 million vehicles reach end-of-life (ELVs) in the United States, generating over 32 million tons of reclaimable material [8]. End-of-life vehicles typically fall into two categories: premature and natural. Premature ELVs are retired before reaching their full service life due to irreparable damage from accidents, fires, or other incidents, and often retain higher-value components. In contrast, natural ELVs reach the end of their lifecycle through routine wear and tear, leaving behind fewer valuable parts. While some buyers attempt to extend the life of aging vehicles through repair and resale, this is largely contingent on whether repair costs exceed the resale value. Once a vehicle enters the ELV supply chain, it typically moves through one of two dominant recovery pathways in the U.S.: manual disassembly or bulk shredding. Disassemblers such as LKQ (Like, Kind, and Quality)as, Pick-n-Pull, and Pull-A-Part focus on extracting reusable components and selecting recyclable materials, with inventory tracked for resale through digital platforms. In some cases, opportunistic parts

such as copper wiring or aluminum engine blocks are also removed. However, plastic recovery is rarely prioritized due to the labor-intensive extraction process and uncertain value, and extraction costs remain poorly documented. After a holding period that varies by business model, typically ranging from one week to twelve months, vehicles are crushed and sent to shredding facilities. This pathway is visualized in **Figure 1.3**. There, the remaining structure undergoes a de-pollution process to remove fluids and hazardous substances before being processed for material recovery. These inefficiencies in the ELV recycling stream, notably the challenges of recovering mixed plastics from Automotive Shredder Residue (ASR), call for closer examination of the material and economic consequences associated with disposal practices.

At shredding facilities, ferrous metals make up the majority of recoverable output, accounting for approximately 70–75%, followed by non-ferrous metals at around 5%, the remaining percentage of 20-25% is a residual stream known as ASR or "fluff," which constitutes 20–25% [12]. ASR is a heterogeneous mixture composed of heavier materials such as glass and fine metal particles (~25%) and lighter materials like plastics, composites, foams, textiles, carpets, rubber, leather, and dirt (~75%). Due to this complexity, ASR presents major separation challenges, as current industrial technologies are largely incapable of efficiently isolating and recovering the diverse types of plastics it contains. At shredding facilities, ferrous metals make up the majority of recoverable output, accounting for approximately 70–75%, followed by non-ferrous metals at around 5%, the remaining percentage of 20-25% is a residual stream known as ASR or "fluff," which constitutes 20–25% [12].

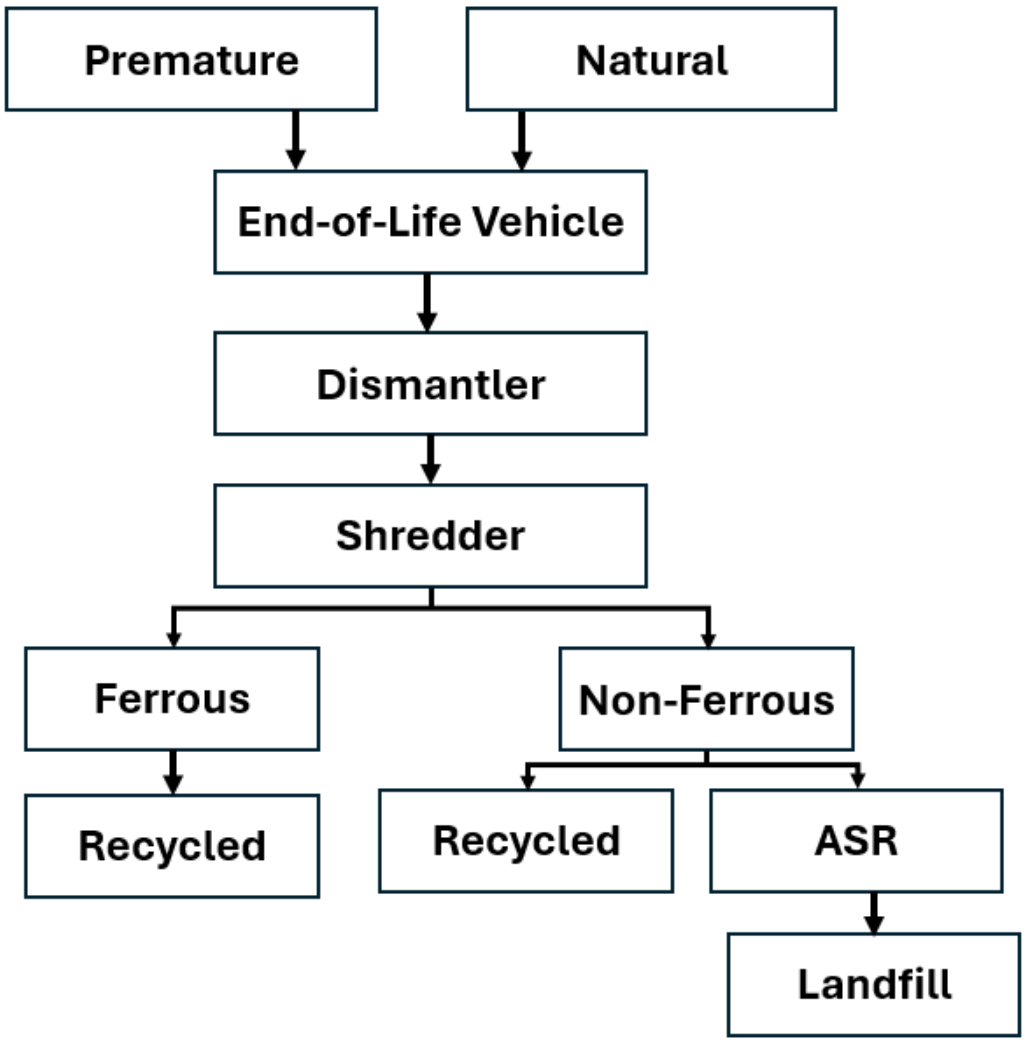


Figure 1.3 - Overview of ELV Recycling Pathway Based on EU Regulatory Directive.

ASR is a heterogeneous mixture composed of heavier materials such as glass and fine metal particles (~25%) and lighter materials like plastics, composites, foams, textiles, carpets, rubber, leather, and dirt (~75%). Due to this complexity, ASR presents major separation challenges, as current industrial technologies are largely incapable of efficiently isolating and recovering the diverse types of plastics it contains.

As a result, the majority of ASR is landfilled, representing a substantial loss of reclaimable polymer content. Among these landfilled plastics, polypropylene (PP) is the dominant contributor by weight, comprising between 24% and 42% of automotive plastic content [8]. These inefficiencies highlight the urgent need for more targeted plastic recovery strategies earlier in the ELV disassembly process, especially in light of rising landfill costs and regulatory pressure.

End-of-Life Vehicle (ELV) Management and Disposal Costs

The continued rise in vehicle ownership is directly tied to an increase in end-of-life vehicles, with an average vehicle life timeline of 18.1 years [13]. In the U.S., the predominant stakeholders in the ELV supply chain include automotive dismantlers and shredders. While dismantlers have found uses for the resale of ELV components, the most widely utilized business model for this industry centers around recycling metal. As a result, the vast majority of plastics, average of 80%, are landfilled at the end of a vehicle's life [14]. Because landfill tipping fees in the U.S. averaged $56.80 per ton in 2023, and vehicles contain an estimated 426 pounds (0.213 tons) of plastic at end-of-life, this translates to an additional disposal cost of approximately $12.10 per vehicle [6, 15]. Considering that approximately 12–15 million vehicles are scrapped annually in the U.S.,

the cumulative cost to shredders from plastic landfill fees alone could amount to up to 181 million USD per year [8, 16]. If it were possible to recover the growing volume of plastics from this EOL supply chain and displace them from the landfill, it could lead to significant cost savings for the ELV supply chain overall.

Policy and Regulatory Landscape

Addressing these recovery challenges requires not only technical solutions but also supportive regulatory structures that incentivize plastic circularity. This shift is further encouraged by evolving regulatory frameworks, such as the European Union's proposed ELV Regulation, which requires that by 2030, all new vehicles contain 25% recycled material, of which at least 25% (equivalent to 6.25% of the total vehicle weight) must come specifically from ELVs [17, 18].

In contrast, the United States currently lacks a national ELV policy or standardized framework for automotive plastic recovery. Most regulations in the U.S. surrounding ELVs focus primarily on metal recycling and hazardous material disposal, leaving plastic recovery largely unregulated and highly dependent on individual state initiatives or voluntary industry efforts. Some U.S. states, such as California, have introduced Extended Producer Responsibility (EPR) programs for other product categories like mattresses and batteries, but automotive plastics are not yet included under these mandates [19]. Internationally, in 2002, Japan enacted the End-of-Life Vehicle (ELV) Recycling Law, which mandates that automakers recover chlorofluorocarbons (CFCs), airbags, and ASR from ELVs, and ensure proper recycling of the remaining vehicle materials [20]. As global sustainability targets intensify, aligning

U.S. regulatory frameworks with best practices from other regions could be key to unlocking broader investment in closed-loop systems for automotive plastics. Current gaps in policy standardization and accountability present a significant barrier to scaling these recycling solutions nationally.

Sequence of Document

The remainder of this thesis is structured as follows: Chapter Two presents a review of the current literature surrounding mechanical recycling methods, life cycle assessment approaches for recycled plastics, and major regulatory and industrial efforts in the ELV sector. Chapter Three outlines the materials and methods used to evaluate the mechanical and thermal performance of recovered plastics. Chapter Four presents the results of mechanical testing, thermal analysis, and material characterization. Finally, Chapter Five discusses the implications of these findings in the context of circular design for automotive plastics and offers recommendations for future research. To contextualize this study, the following chapter first reviews the current state of plastic recycling technologies and life cycle assessment methods used to evaluate environmental impacts.

CHAPTER TWO

LITERATURE REVIEW

Building on the need to divert plastics from landfills and reduce ELV-associated waste, Chapter Two explores the landscape of available recycling technologies, their constraints, and their integration into automotive supply chains. Several recycling technologies have been explored for processing plastics from ELVs, including mechanical, thermal (i.e., pyrolysis), chemical (i.e. solvolysis), and enzymatic/biological methods. For example, in mechanical recycling, parts are shredded and directly remanufactured or sometimes pelletized and reused in manufacturing. Thermal recycling technologies, such as pyrolysis, involve the thermolytic decomposition of plastics in the absence of oxygen. Enzymatic and biological recycling methods use specialized enzymes or microbes, such as bacteria or fungi, to selectively depolymerize polymers like polyethylene terephthalate (PET), breaking them down into monomer building blocks under mild, biologically driven conditions[21]. Pyrolysis, a chemical technique, has emerged as a leading approach. It produces pyrolysis oil that can be refined into fuels or used as a chemical feedstock [22]. This approach is especially suited for polyolefins like PA and polyethylene (PE), materials that are otherwise not compatible with solvent-based recycling methods [23]. Eastman Chemical Company has already established a commercial-scale pyrolysis facility in Kingsport, Tennessee, while ExxonMobil is investing heavily in expanding its Exxtend pyrolysis program, which aims to process up to one billion pounds of plastic waste annually by 2027 [24, 25].

Solvolysis, including metanalysis and glycolysis, represents another pathway being explored at scale, particularly for condensation polymers like PET [26]. In this process, solvents are used to depolymerize plastics into their monomer building blocks, which can then be repolymerized into high-quality materials. Eastman is also advancing this method with a new metanalysis facility under construction in France, expected to handle 160,000 tons of plastic waste annually by 2025 [27]. However, solvolysis is inherently limited to a narrow class of polymers and is not suitable for most polyolefins or vinyl-based plastics due to their highly stable carbon–carbon backbones and the potential for releasing harmful byproducts [28].

Enzymatic recycling, is a promising option in polymer recovery, particularly for PET. This method employs specialized enzymes like PETase and MHETase that catalyze the depolymerization of PET into its original monomers, such as terephthalic acid and ethylene glycol, under relatively mild conditions [29]. Companies like Carbios are new industrial applications of this approach, though enzymatic recycling remains limited in scope and is not yet applicable to the most common automotive polymers, such as PE, PP, or PVC, due to their structural resistance to enzymatic attack [30]. Another effort to address contamination in mechanically recovered plastics came from ECO2 Plastics, Inc., which piloted a closed-system cleaning process using a biodegradable biosolvent followed by liquid carbon dioxide treatment. Funded by the Vehicle Recycling Partnership (VRP), this method was specifically designed to remove PCBs from polyolefin-rich shredder residue [31]. The process involved distillation-based recovery of solvents and collection of extracted contaminants. According to the ECO2 final report,

testing using extended Soxhlet extraction and GC/MS analysis showed no detectable PCBs, suggesting potential for cost-effective implementation at commercial scale [31]. A visual of these pathways can be seen in **Figure 2.1.**

While thermal, chemical, and enzymatic recycling technologies offer promising potential for future circular material flows, they are currently constrained by high energy demands, lower material compatibility, and often lower technology readiness levels [32]. For these reasons, mechanical recycling remains the most widely implemented technology due to its scalability and energy efficiency [33].

In industrial mechanical recycling, companies will recover plastics, use physical methods to clean and separate contamination from the waste stream, and directly re-use the material to make new pellets for manufacturing [34]. A recent life cycle assessment conducted using Gabi software found that producing PP pellets from recycled plastic waste can result in approximately 41.8% lower carbon emissions than virgin PP, depending on solvent recovery and energy source [35]. For now, mechanical recycling offers the most practical path for reintegrating recovered plastics into new vehicle components, especially when disassembly and sorting are optimized [36]. Because it preserves the polymer backbone and relies on physical reprocessing rather than chemical transformation, mechanical recycling is particularly effective for relatively clean, homogenous plastic streams, such as those recovered through disassembly of ELV components [37]. To quantify the environmental performance of these recycling technologies and guide material selection, life cycle assessment (LCA) has become an essential decision-making tool in both industry and academia.

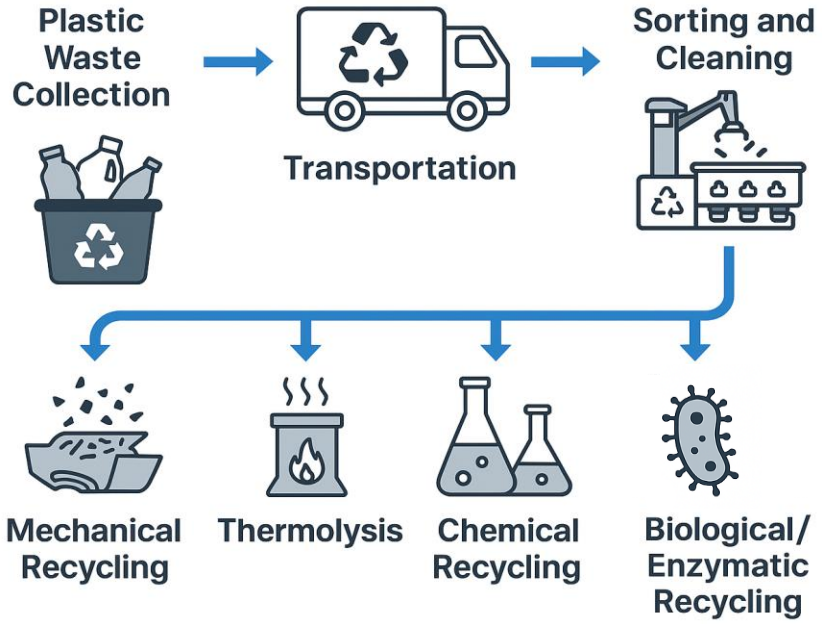


Figure 2.1 - Overview of Plastic Recycling Technologies and Their Suitability for ELV Waste Streams adapted from Jiang. X et al.

Life Cyle Assessment Frameworks

To better evaluate the environmental benefits of these recycling pathways, researchers often rely on Life Cycle Assessment (LCA) frameworks. LCAs quantify the environmental impacts associated with a product's life stages, from raw material extraction to disposal, and are particularly useful for comparing virgin versus recycled plastic streams[38]. Within LCA modeling, two common allocation methods used in life cycle assessments of recycled plastics are the cut-off method and the open-loop method, both of which are accepted under ISO 14044. In most comparative LCAs that assess the benefit of recycled content in product manufacturing, the cut-off method is typically preferred, as It assigns the environmental burden of virgin production solely to the first use, with only recovery and reprocessing burdens attributed to the recycled product. The open-loop method, by contrast, divides the burdens of virgin production and recycling operations across multiple useful lifespans of the material. While both methods are useful for different modeling goals, the cut-off approach is more commonly used in studies focused on highlighting impact reduction from material substitution[39]. Despite the usefulness of LCA in quantifying potential benefits, achieving these environmental gains in practice depends heavily on the feasibility of recovering and reprocessing ELV plastics. However, the recovery of ELV plastics is often hindered by economic and design constraints. Manual disassembly and part complexity remain key hurdles, making it difficult to isolate clean, homogeneous polymer streams suitable for recycling. Even when technically feasible, these materials may require expensive reprocessing to meet automotive performance standards. Contaminants such as residual paint particles can

compromise the impact strength of recycled parts, further reducing the economic viability of ELV plastics as feedstock [8].

Barrier to ELV Plastic Recovery

As previously noted, these technologies remain constrained by energy requirements and compatibility issues, limiting their near-term scalability. As a result, mechanical recycling continues to be the most accessible route for integrating recycled plastic content into the automotive sector particularly when paired with improved disassembly and material separation practices at the ELV stage.

While there is technical potential for recovering plastic components from ELVs, significant barriers have limited large-scale adoption in the U.S. automotive sector. Past efforts by OEMs to reclaim TPO from post-industrial bumpers using chemical and high-pressure steam paint removal processes ultimately proved cost-prohibitive and were discontinued [8]. Building on prior challenges, including contamination, labor cost, and inconsistent supply, mechanical recycling now emphasizes clean, segregated input streams for viability. Despite these past challenges, the market landscape is shifting. OEMs now face regulatory and corporate sustainability pressures to integrate recycled plastic into new vehicle designs by 2025 or 2030, creating new momentum for circular strategies. Automotive disassemblers, who already operate highly organized recovery systems where each removed part is labeled and digitally tracked, are uniquely positioned to enable scalable ELV plastic recovery. However, realizing this potential will require targeted design guidance from OEMs, financial incentives from policy makers, and coordinated efforts across the supply chain. As past efforts have shown, no single

stakeholder can overcome the logistical and economic barriers alone. But with OEMs increasingly prioritizing recycled content to meet sustainability goals, and recyclers facing growing pressure to diversify value streams, there is a timely opportunity to align disassembly practices with circular material flows and unlock new economic and environmental value from end-of-life plastics [8]. Despite these challenges, a number of automotive manufacturers have launched initiatives aimed at integrating recycled plastic into vehicle production, with varying degrees of success.

Automotive Industry Attempts to Recycle Plastics

Manufacturers have initiated various strategies to meet growing regulatory and sustainability targets related to recycled content in vehicles. Ford Motor Company initiated the use of 100% recycled ocean plastics for wiring harness clips in the Bronco Sport and replacing petroleum-based materials with soy-based foam for seat cushions [40]. Jaguar Land Rover incorporates Econyl nylon, sourced from recycled industrial plastic, fabric offcuts, and abandoned fishing nets, into its vehicle interiors [41]. BMW's i3 model features door panels made from hemp fibers, reducing weight and improving sustainability [42]. Additionally, Volvo's EX30 SUV operates a combination of recycled denim, flax, and a wool blend with approximately 70% recycled polyester across its upholstery, dashboard, and door panels [43].

Other manufacturers are focusing directly on plastics recovered from scrapped vehicles. Honda and Nissan are developing supply chains aimed at recycling plastics from ELVs, with the goal of enhancing the recyclability of automotive plastics and reducing environmental impact. Honda, in particular, has partnered with Idemitsu Kosan

to chemically recycle collected plastic into oil, which can then be used to manufacture new materials with performance comparable to virgin plastics [44]. Audi, in collaboration with LyondellBasell, has launched the PlasticLoop Project, a closed-loop initiative focused on chemically recycling mixed automotive plastic waste [45]. The process involves dismantling plastic components from customer vehicles that can no longer be repaired, followed by shredding and converting them into pyrolysis oil through advanced chemical recycling. This oil is then used as a raw material to manufacture new plastic components, such as seatbelt buckle covers featured in the Audi Q8 e-tron [45]. In parallel, the ELV Project, launched by the Plastics Industry Association in 2015, focused on recovering thermoplastic polyolefin (TPO) bumpers from ELVs using mechanical processes such as shredding, magnetic separation, elutriation, and extrusion [46]. While the recycled material retained 85–90% of the mechanical properties of virgin TPO, the project faced major scalability challenges due to contamination, inconsistent bumper collection logistics, and high processing costs [46]. These initiatives demonstrate both the feasibility and the current limitations of incorporating recycled plastics, especially from post-consumer sources like ELVs.

To illustrate the application of mechanical recycling at scale, one example of is MBA (Michael Biddle & Associates) Polymers, which processes up to 80,000 metric tons of plastic-rich shredder residue annually, including ELV-derived material, at its facilities in the UK and Austria [47, 48]. Their mechanical recycling process uses density separation, flotation, and electrostatic sorting to extract polymers such as PP and acrylonitrile butadiene styrene (ABS), typically achieving 85–90% purity [48]. While

industrial initiatives provide proof-of-concept examples, academic research is essential to evaluate material performance, standardize methods, and identify viable pathways for broader adoption.

Academic Research Models

Academic literature in the physical characterization & recycling of plastics obtained directly from ELVs is limited. While several recent publications have explored the use of recycled composites in automotive components, they have not obtained these components directly from ELVs and instead used manufacturing scrap for recycling demonstrations [32-35]. Therefore, it is not clear how the functional use life of these materials will impact their recyclability as the use of life plastics can significantly impact their performance [31, 36]. Others have attempted to simulate the use-life using thermal aging, but it is not clear whether these methodologies will accurately show the functional use life degradation of these materials where they may experience UV-degradation, humidity, and even be painted [6, 37]. While there are publications which have sought to characterize the automotive shredder residue stream, [38] to the best of the authors' knowledge, disassembled ELV plastics characterization is limited. In 2024, Juan et al. explored the use of disassembled bumpers from ELVs, but the heterogeneity in ELV bumpers may present a barrier to recyclability in concentrations above 50% in new parts. [39] However, beyond this single example it is not yet clear how much residual performance remains in unpainted ELV plastics throughout the ELV assembly when obtained from the automotive disassembler.

Objectives of the Present Study

This study explored the recovery and recycling of disassembled plastics obtained throughout ELVs in multiple unpainted components. Working with the automotive supply chain, industrially sourced control samples were used to quantify and evaluate the effects of a vehicle's service life on the mechanical properties of plastic components at end-of-life. ELV plastics were subjected to mechanical recycling, and the impact of the recycling process on their mechanical performance in secondary, injection molded test samples was assessed. The results of this work represent a significant step toward enabling a circular economy for automotive plastics by providing data-driven insights into the viability of closed-loop recycling for disassembled vehicle materials.

CHAPTER THREE METHODS AND MATERIALS

Materials

Four model materials were obtained from LyondellBasell (LB) to represent the disassembled ELV plastics used in this study. *Adstif* HA801U (32004857) a neat polypropylene homopolymer, was selected to represent the virgin baseline material for the bumper fascia component. *Sequel* 2326 Natural (1A791), a mineral-filled polyolefin compound, was used as the virgin material for the rear deck trim cover and is referred to as PP-T10 throughout this study. *Hifax* TYC 1235X Black (1BG24), PP homopolymer filled with 22% talc by weight, was used to represent the trunk interior panel and is referred to as PP-T20 in this work. Lastly, FP62E15 (PA6 GF15) (1E8M7), a nylon 6 compound reinforced with approximately 15% mineral fillers including 10-30% fiber and 1-5% carbon black by weight, was selected to match the engine cover known as PA6+GF7+MF13 in this study. These materials were chosen based on identification labels found on the ELV components and were verified using the manufacturer safety data sheets (SDS). For clarity and consistency, the simplified names of (virgin) PP, PP-T10, PP-T20, and PA6+GF7+MF13 are used throughout the remainder of this paper.

ELV Disassembly

Four thermoplastic, unpainted ELV components were manually disassembled at an automotive scrapyard. These included a bumper fascia (PP), a trunk interior panel (10% talc PP by weight), a rear bumper extension (20% talc PP by weight), and an engine cover. (20% GF/MF nylon by weight). At the disassembler, these plastic components were sitting in the remaining “husk” of the vehicle after valuable components had been

removed using heavy machinery. Plastic components were not attached to the vehicle and were facile to isolate and remove from the ELV. This is shown in **Figure 3.1**. As shown in **Figure 3.2**, each component removed was molded with a label embedded that included useful information about the material, original equipment manufacturer (OEM), location of manufacturing, and a lot number. The labeling allowed the identification of each part's polymer formulation, which was then matched to equivalent virgin-grade materials obtained from LyondellBasell to represent the components at the beginning of their use life.

Sample Preparation

The mechanical recycling process followed in this work is visualized in **Figure 3.3**. ELV parts obtained from the scrapyard were found to be dusty and dirty from having sat outside in the lot for at least 1 week. Four automotive plastic components were cut into approximately 11cm x 3cm sections using a bandsaw to ensure compatibility with the shredding equipment. To minimize contamination in the samples, all components were washed with soap and water by hand and sponge and dried at 65°C for at least 24 hours.

Dried parts were shredded using a GP20 Plastic Shredder (3Devo - Utrect, NL, EU) operating at 14 RPM, within a chamber temperature range of 26–32 °C. The shredder is equipped with an internal mesh screen that limits particle size to below 4 mm, producing consistent and process-ready granules suitable for injection molding see **Figure 3.4**. To eliminate contamination, the equipment was disassembled and cleaned using a wet/dry vacuum between the materials.

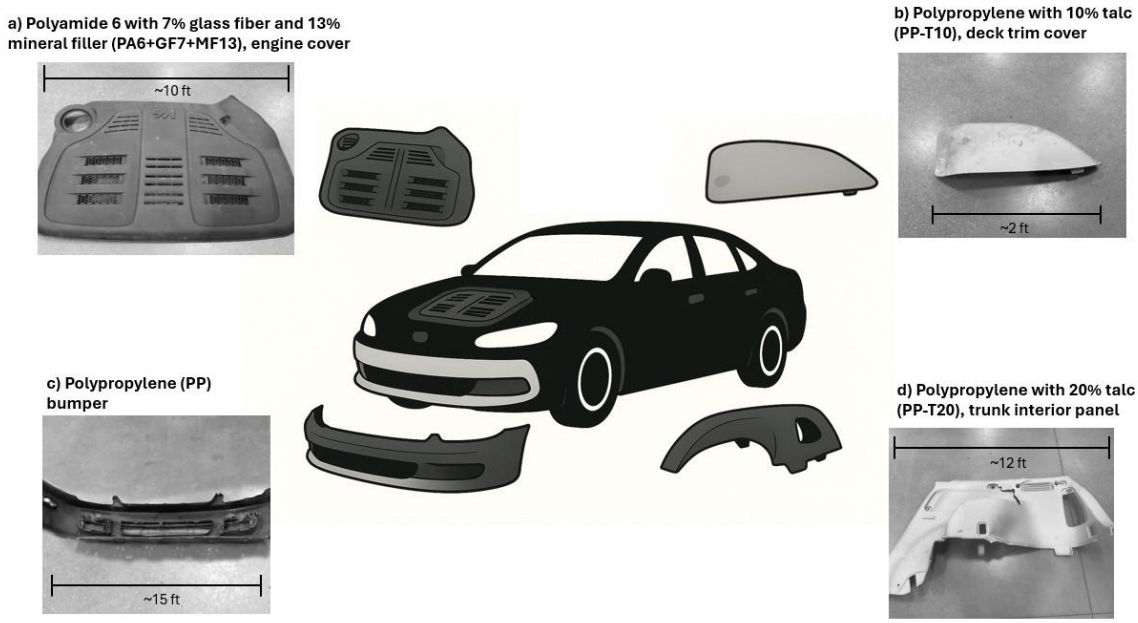


Figure 3.1 Photographic overview of disassembled end-of-life vehicle (ELV) components selected for mechanical recycling. Four thermoplastic parts were manually recovered from a vehicle and identified by their embedded material markings: (a) engine cover (PA6+GF7+MF13), (b) deck trim cover (PP-T10), (c) front bumper fascia (PP), and (d) trunk interior panel (PP-T20).The central illustration maps the approximate location of each part on the vehicle.

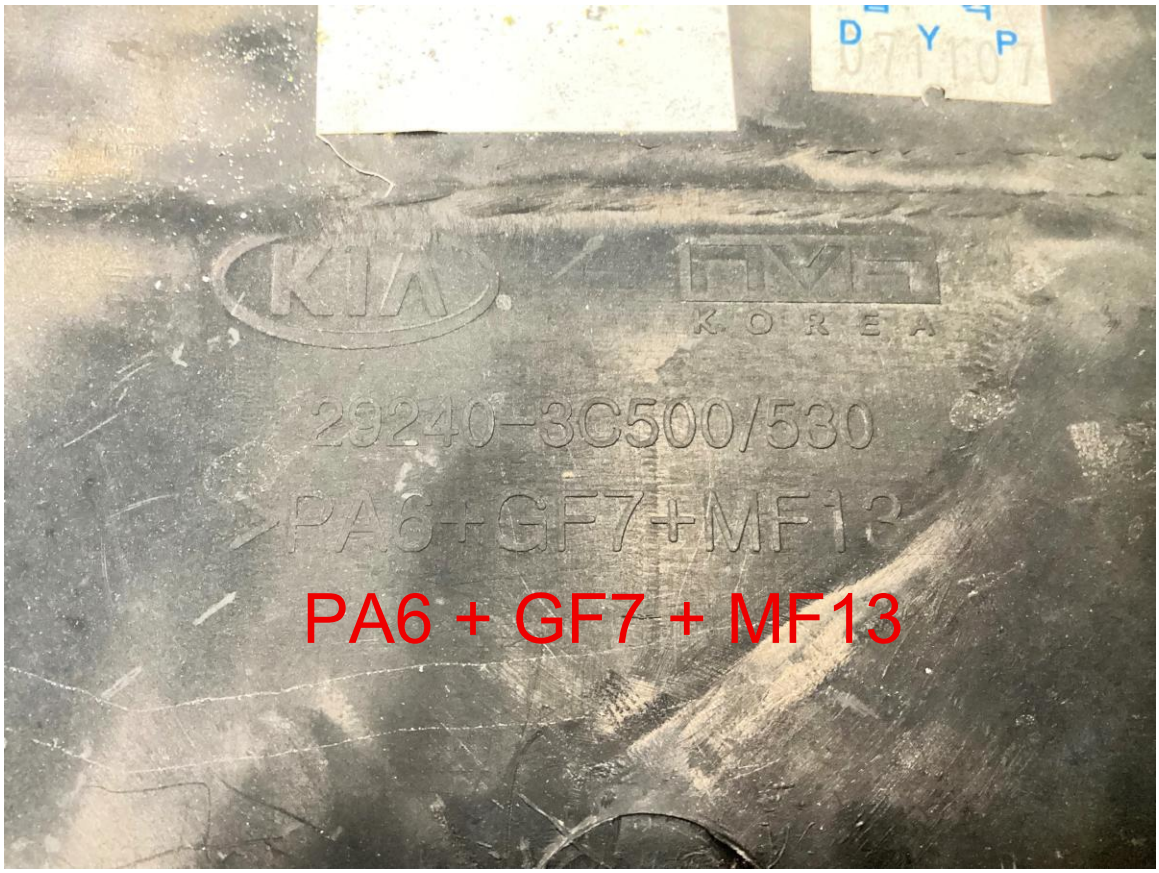


Figure 3.2 Close-up image of embedded part labeling on the disassembled engine cover. The molding indicates the material (PA6+GF7+MF13), the manufacturer Kia, and the original part number, allowing identification and tracking of the base polymer and filler content.

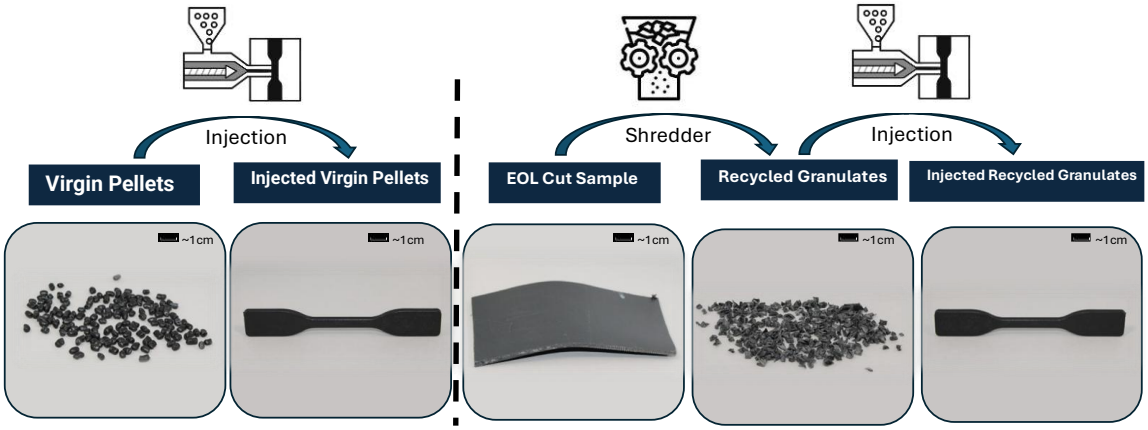


Figure 3.3 - Visualization of the process pathway for mechanical recycling of EOL vehicle plastics.

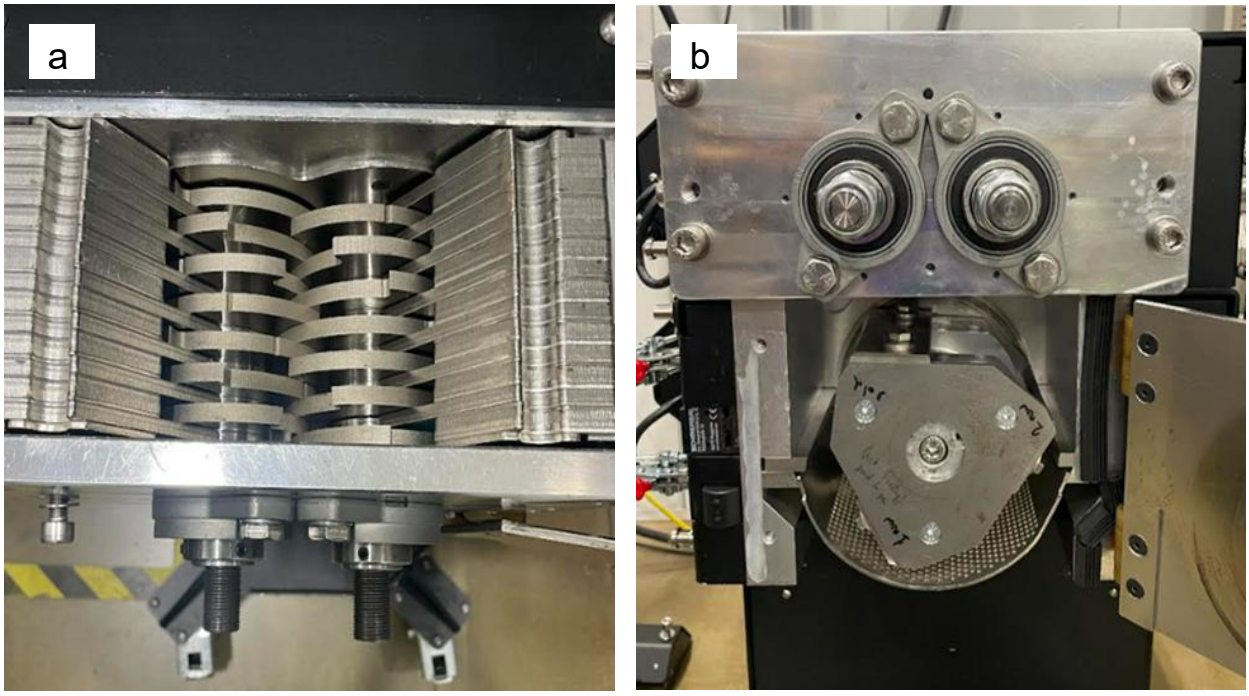


Figure 3.4 Internal views of the GP20 plastic recycling system. (a) Shredder chamber showing the interlocking combs and rotating blades used to break down large polymer parts. (b) Granulator unit with a rotating cutting blade and cylindrical mesh screen used to achieve consistent particle sizing below 4 mm.

Two collection methods were used to recover the shredded granulate. A stainless-steel bin was positioned at the base of the shredder with a collection bag taped in to capture the bulk of the material as it was discharged. Additional granules that accumulated in the equipment chamber were manually vacuumed into labeled plastic containers. To evaluate material recovery efficiency during the shredding process, mass input and output were tracked for each selected ELV component. Each part was weighed prior to shredding, and the resulting granulate was divided into two fractions: material captured directly in the hopper and material manually recovered by vacuum. A small portion of mass loss to the equipment was also recorded. To account for differences in starting mass, granulate recovery values were normalized to the initial feedstock weight for each sample. As shown in **Figure 3.5** and **Table 3.1**, most samples demonstrated high recovery efficiency (>90%), with vacuum recovery varying based on the static behavior of the material.

After shredding, the granules were dried again in a convection oven at approximately 150 °C for at least 24 hours to ensure uniform moisture removal. The 4 model materials obtained from LyondellBasell and the 4 granulated samples were then injection molded into standardized ASTM D638 Type V dogbone test bars using an APSX-PIM V3 Plastic Injection Machine (APSX, Blue Ash, OH, USA). Granulated samples were used as feedstock for re-manufacturing to minimize material degradation associated with the compounding process that would be required to make pellets.

For PP materials, the barrel temperature maintained between 220–230 °C and the mold temperature around 80 °C. Injection pressure was maintained at 180 bar, and an

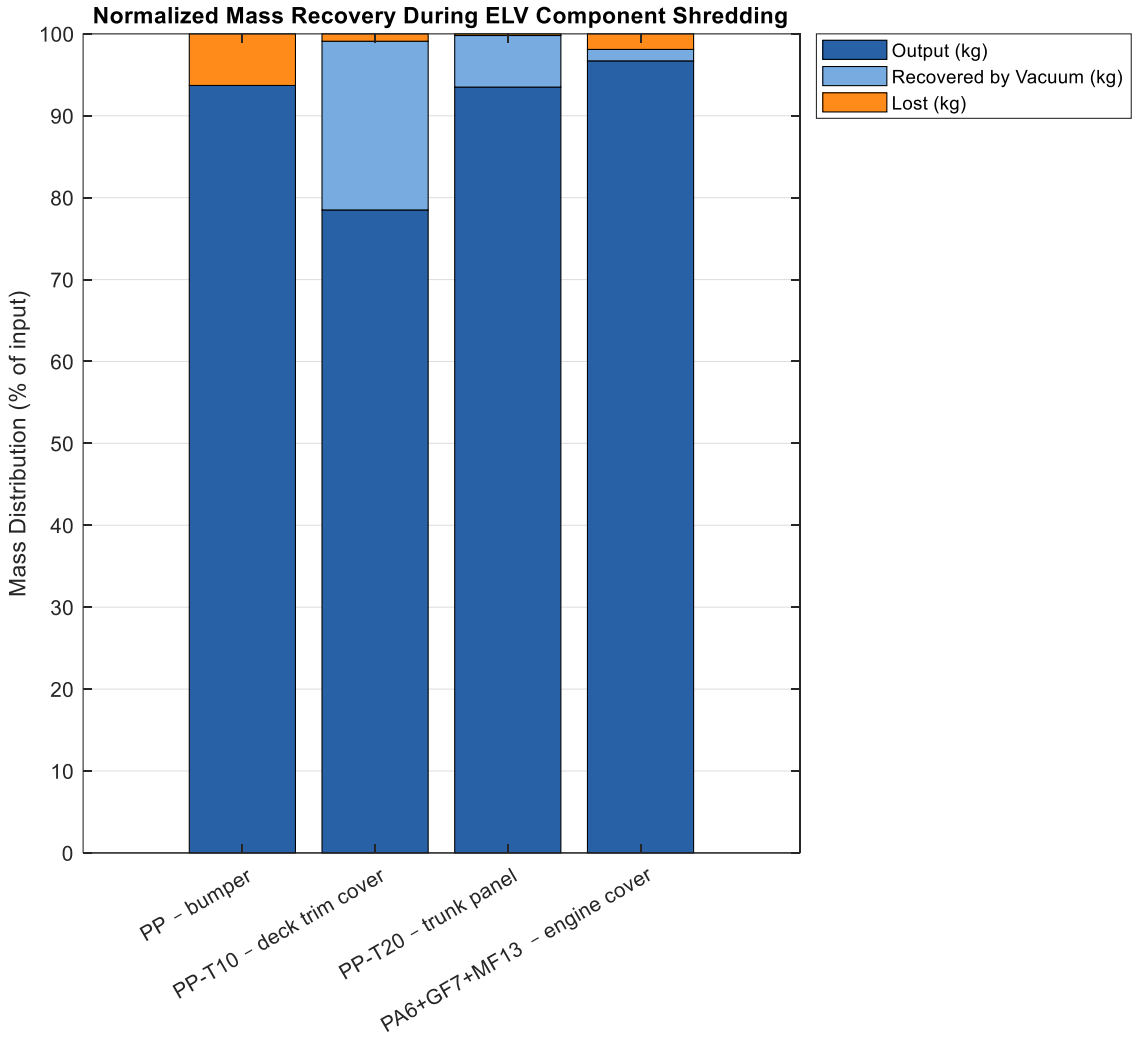


Figure 3.5 - Normalized material recovery breakdown by polymer and ELV component. Bars represent the mass distribution of each sample as a percentage of its starting feedstock. Recovered material is divided into portions captured directly in the hopper and manually recovered by vacuum, with the remaining mass attributed to shredding loss. Components include a bumper (PP), deck trim (PP-T10), trunk panel (PP-T20), and engine cover (PA6+GF7+MF13).

Table 3.1 - Mass flow data for shredded ELV samples. For each part, the table includes the original feedstock weight, total granulate collected, the portion recovered by vacuum, and estimated material loss during shredding. A dash (–) indicates no record was taken.

			Collected Sample (kg)			Lost Sample (kg)	
Car Part	**Material**	**Feedstock (kg)**	**Output (kg)**	**Vacuum (kg)**	**Total %**		**Total %**
Bumper	PP	4.22	3.95	-	93.7	0.063	1.5
Deck Trim Cover	PP-T10	0.16	0.13	0.03	94.8	0.009	5.4
Trunk Interior Panel	PP-T20	0.93	0.87	0.06	99.4	0.003	0.3
Engine Cover	PA6+GF 7+MF13	1.23	1.21	0.02	99.0	0.004	0.4

additional hold pressure of 150 bar was applied during the cycle. The machine operated with a clamp force of approximately 3775 kg. For PA samples, a higher barrel temperature range of 260–288 °C was used, with a mold temperature of approximately 102 °C. The injection pressure was maintained between 190–220 bar. Each molding cycle used a hold time of 10 seconds, a cooling time of 25 seconds, and a clamp time of 30 seconds. The total injected material per cycle was around 10.6 cm^3. After molding, all test specimens were cooled at ambient room temperature prior to further testing.

Characterization

The following section outlines the various characterization methods used to evaluate the physical, thermal, and chemical properties of the selected materials.

Particle Size Analysis

Particle size analysis was conducted using a custom image-based measurement system developed at ORNL. The setup consisted of a Logitech BRIO 4K Ultra HD webcam mounted over a white background, connected to a Dell Precision 3650 desktop computer. Sample trays containing recycled granules or virgin pellets were photographed under consistent lighting conditions. The images were processed using a Python-based image analysis tool, chromatology, developed by ORNL researchers. The software uses the opencv-python package to segment and identify individual particles, fit bounding rectangles around each one, and export key size metrics (e.g., area in mm^2) into CSV files for further analysis.

For each material group, five replicate batches around 100 pieces each were scanned and exported as CSV files containing individual particle areas in mm^2. Data

processing was performed in MATLAB (MathWorks, MA, USA). The area values from each batch were combined and filtered to exclude particles above 300 mm^2 to eliminate agglomerates and outliers. Histograms were generated using 10 mm^2 bin widths, and the mean and standard deviation of particle area were calculated. For each group, 95% confidence intervals were computed using the normal distribution ($z = 1.96$), based on the standard error of the mean.

Density

The density of the samples was measured using a Micromeritics AccuPyc 1340 II pycnometer with hydrogen gas. Each sample was cut from a small testing bar and weighed between 0.2 and 0.5 grams, and each formulation was tested three times to ensure accuracy. The sample volume (cm^3) and density (g/cm^3) were recorded over five cycles, and the average and standard deviation were calculated for each sample to facilitate comparison.

FTIR

Fourier-transform infrared (FTIR) was performed using a Nicolet iS50 FTIR Spectrometer (Thermo Scientific, Waltham, MA, USA) outfitted using a diamond crystal to compare the chemical structure of injection molded virgin pellets and injection molded recycled granules samples. Spectra were acquired in the range of 500 to 4000 cm^{-1} and subsequently processed using Origin software. Raw absorbance data were normalized between 0 and 1 to allow direct comparison of peak intensities. Normalized spectra were then plotted using stacked views to visually separate the virgin and recycled curves while

maintaining the same x-axis scale. Plot appearance, including curve color, thickness, axis range, and text, was manually adjusted for clarity and consistency. All FTIR peaks were interpreted as relative to known characteristic absorbance bands for PP and talc-filled composites.

TGA

Thermal stability of the composites was evaluated using thermogravimetric analysis (TGA) on a TGA Q500 (TA instruments, New Castle, DE, USA) . Samples were heated from room temperature to 600 °C at a rate of 10 °C/min under argon flow at a sample purge flow rate of 10 mL/min. The onset degradation temperature (T_{onset}) and temperature at maximum weight loss (T_{max}) were recorded from the first derivative of the mass loss curve (DTG). Each test was conducted in triplicate for all material types to ensure repeatability. The data was used to compare thermal stability between materials and to assess whether degradation onset shifted between recycled and virgin samples.

DSC

DSC measurements were performed on a TA Instruments Q2000 according to ASTM D3417 using approximately 5 mg of material in sealed aluminum pans. Thermal transitions and crystallinity were characterized. The scanning conditions were set as follows: Samples were heated from room temperature to 250 °C at 10 °C/min, equilibrated at 250 °C, then cooled to 0 °C at 10 °C/min equilibrated at 0 °C and subsequently heated again to 250 °C at 10 °C/min.

The degree of crystallinity (X_c) was calculated from the first heating cycle using Equation 1:

$$X_c = \frac{\Delta H_m}{w \times \Delta H_{100}} \quad (1)$$

In which ΔH_m is the melting enthalpy, w is the weight fraction of PP or PA in the composite (e.g., 0.8 for 20% talc-filled PP), and ΔH_{100} is the melting enthalpy for 100% crystalline polymer. A value of 207 J/g was used for PP based on literature [49] and 230 J/g for PA based on literature [50]. All DSC runs were performed in triplicate for each sample type to ensure accuracy and reproducibility of the thermal transitions.

HDT

The small compression-molded bars were used in a DMA 850 (TA Instruments DE, USA) to find the HDT values for a low-stress (0.455 MPa) three-point bend test. Three bars were tested for each sample with the temperature going up to 74°C, and the force (ranging from ~0.7-1.2) was calculated based on the length, width, and thickness.

Mechanical Testing

Dog-bone specimens (ASTM D638 Type V) were tested at room temperature using Instron 5965 Universal Testing System with 5 kN Pneumatic Side Action Tensile Grips see **Figure 3.6**. Each sample was tested at a rate of 5-10 mm/min. A minimum of 4 specimens were tested for each sample type. At least four specimens per sample were tested, and the average tensile strength, and Young's modulus were reported.



Figure 3.6 ASTM Type V dog bone sample mounted for tensile testing in an Instron universal testing machine.

CHAPTER FOUR

RESULTS AND DISCUSSION

This section presents the experimental results from physical, mechanical, and thermal characterization of four polymer formulations across various processing stages: virgin, end-of-life (EOL), granulated, and recycled-injection molded. The results include particle size analysis, density, crystallinity, chemical structure, thermal stability, mechanical performance (Young's modulus and UTS), and heat deflection temperature (HDT), with figures organized by material and property for clarity.

Particle Size Analysis & Sample Density

Particle size analysis was performed on both virgin pellets and recycled granules (**Figure 4.1a**). As can be seen, virgin pellet particles were larger and more uniform in distribution (μ =155.1 ± 102.26 mm^2), with some small dust particles contained in the batch. However, the recycled granule samples had a much broader particle size distribution with a significantly lower particle size on average (μ = 71.9 ± 64.2 mm^2, a 53% average reduction over virgin pellets). Previous literature has shown that directly re-manufacturing thermoplastic granules can have the minimum impact on the material properties overall but can result in parts that have reduced density due to decreased stacking efficiency [51]. To quantify any changes in resulting density of the parts, samples were analyzed using pycnometry (**Figure 4.1b**). As can be seen, small changes in the resulting densities were observed between injection molded virgin and recycled PP, PP-T20, and PA6-GF7-MF13 samples. In the case of neat PP, injection molded samples made from recycled granules (0.95 ± 0.01) saw a significant (5%, $p<0.05$) increase in

density over samples made from virgin pellets (0.91 ± 0.01). However, for PP-T20 and PA6-GF7-MF13 samples, a 4.7% reduction and a 2.4% increase in average density were observed respectively ($p<0.05$). Though there are small, statistically significant changes in the average density of injection molded parts, there is no clear trend in either direction observed in recycled samples. Therefore, it is unlikely that small changes observed in density between samples were directly caused by the difference in particle size observed between recycled granules and virgin pellets. FTIR was performed to confirm whether these changes were visualized because of differences in model formulations obtained by LyondellBasell and ELV components, which is shown in the FTIR section of this document. These results suggest that particle size has limited impact on resulting part density, supporting the use of granules as a more cost-effective injection molding feedstock without compromising quality [8]. Additionally, it becomes evident that some differences observed between virgin and recycled parts may stem from formulation mismatches.

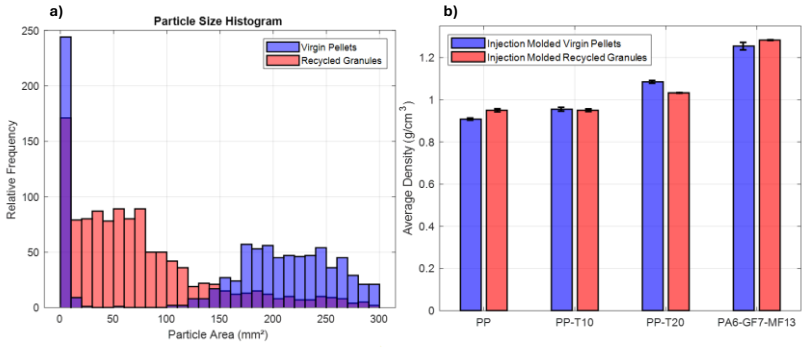


Figure 4.1- a) Particle Size Analysis of both granulated and virgin pellet samples. b) Average density of injected molded parts made from both virgin pellets and recycled granules.

Fourier Transform Infrared Spectroscopy (FTIR)

FTIR spectroscopy was used to qualitatively compare the chemical structure of injection molded pellets and injection molded recycled for all four formulations. This analysis was intended to identify any visible changes in characteristic functional group regions, such as oxidation products or additive signatures that may arise during service life or reprocessing. FTIR spectra for PP, PP-T10, PP-T20, and PA6+GF7+MF13 are presented below.

FTIR spectra of injection molded virgin and recycled PP (**Figure 4.2**) reveal consistent peaks associated with C–H stretching (around 2950–2800 cm^{-1}) and CH_2 bending (1460 and 1375 cm^{-1}), which are characteristic of the PP backbone [50]. However, a noticeable shift and broadening near 1450 cm^{-1} is observed in the recycled sample, which may indicate the presence of an additive or stabilizer introduced during the original product's manufacturing or post-use life. This peak is absent in the virgin material and may reflect a chemical modification or formulation difference in the recycled material. Additionally, a more distinct single peak near 1000 cm^{-1} is observed in the recycled PP spectrum whereas there appear to be 2 distinct peaks in this region in the virgin sample.

This single peak may be attributed to unsaturated chain ends, specifically C–H bonds adjacent to unreacted C=C double bonds, which can form through oxidative degradation or incomplete polymerization [52]. This difference in spectra could also be attributed to an additive in the PP, as peaks near $1000cm^{-1}$ could be indicative of C-O bond stretching[53]. The observed differences in FTIR spectra between virgin and

recycled PP may also be attributed to differences in tacticity [54, 55]. Tacticity refers to the stereoregularity of the polymer chain, specifically the spatial arrangement of the methyl groups (–CH_3) along the backbone. An isotactic PP would yield 2 peaks 974 and 995 cm^{-1}, consistent with what is observed in the virgin PP spectra. In contrast, the recycled PP obtained from ELVs could be more indicative of atactic PP, with randomly oriented methyl groups resulting in a single peak around 974 cm^{-1} [56].

The FTIR spectra of PP-T10 (**Figure 4.3**) exhibit characteristic PP absorption bands for both injection molded virgin and recycled samples. Major peaks associated with C–H stretching (2950–2800 cm^{-1}) and CH_2 bending (1455 and 1375 cm^{-1}) are retained across both spectra, indicating that the core polymer structure remains largely intact. However, a new broad peak appears near 3500 cm^{-1} in the recycled PP-T10 sample, which is indicative of O–H stretching. This feature is absent in virgin material, suggesting water contamination or absorption may have occurred during the recycling workflow. The FTIR spectra for PP-T20 (**Figure 4.4**) samples show retention of key PP vibrational peaks in both virgin and recycled conditions. Similar to PP-T10 a broader peak appears near 3500 cm^{-1} indicative of O–H stretching, suggesting water contamination. The FTIR spectra of PA6+GF7+MF13 (**Figure 4.5**) , both virgin and recycled samples display strong amide I (around 1640 cm^{-1}) and amide II (around 1540 cm^{-1}) bands characteristic of the PA backbone [57]. Apart from minor differences in peak intensity and baseline variation in the recycled sample, overall peak assignment and shape remain largely consistent between samples.

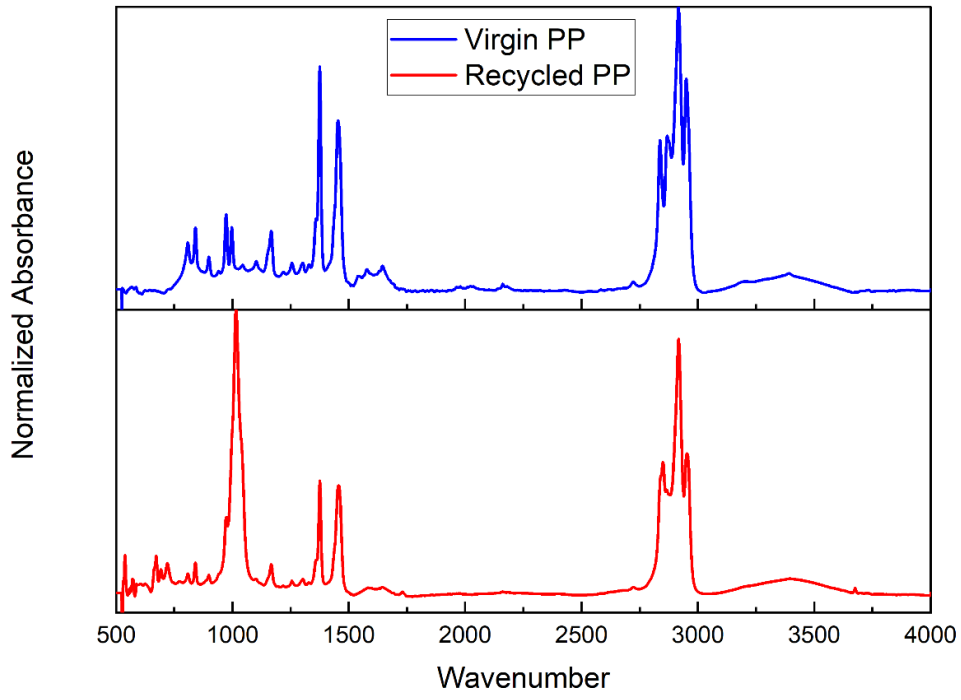


Figure 4.2 - FTIR spectra of injection molded virgin PP pellets and injection molded recycled PP granules

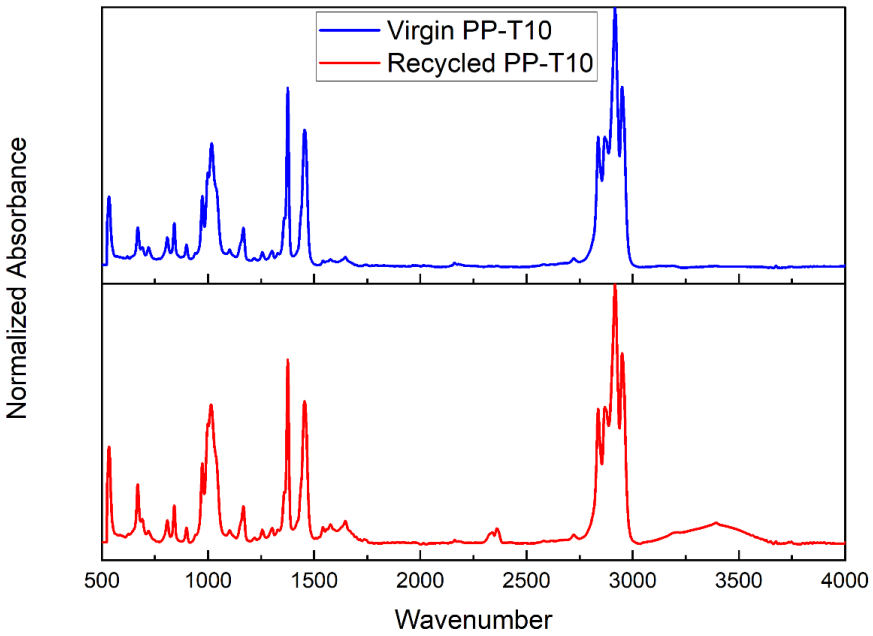


Figure 4.3 - FTIR spectra of injection molded virgin PP-T10 pellets and injection molded recycled PP-T10 granules.

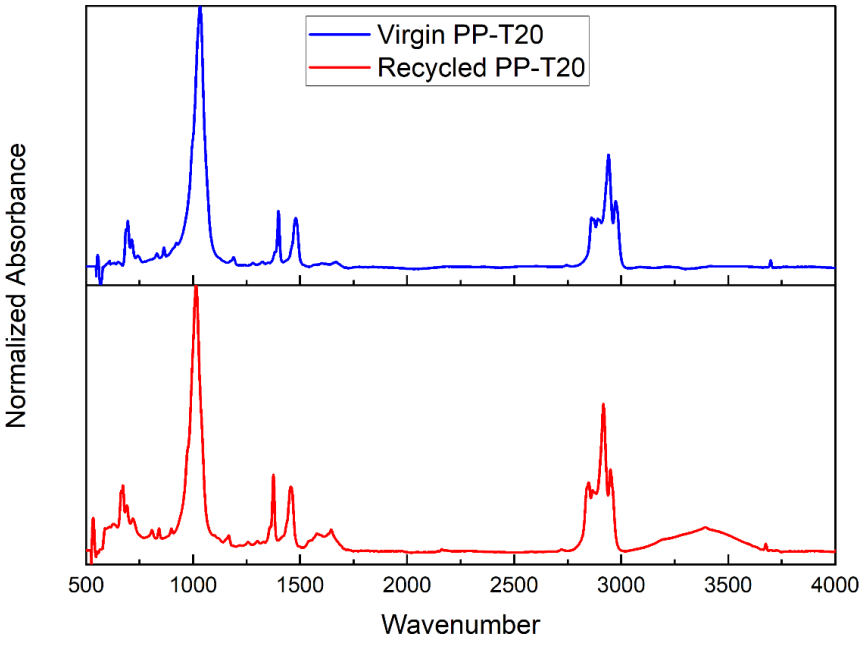


Figure 4.4 - FTIR spectra of injection molded virgin PP-T20 pellets and injection molded recycled PP-T20 granules

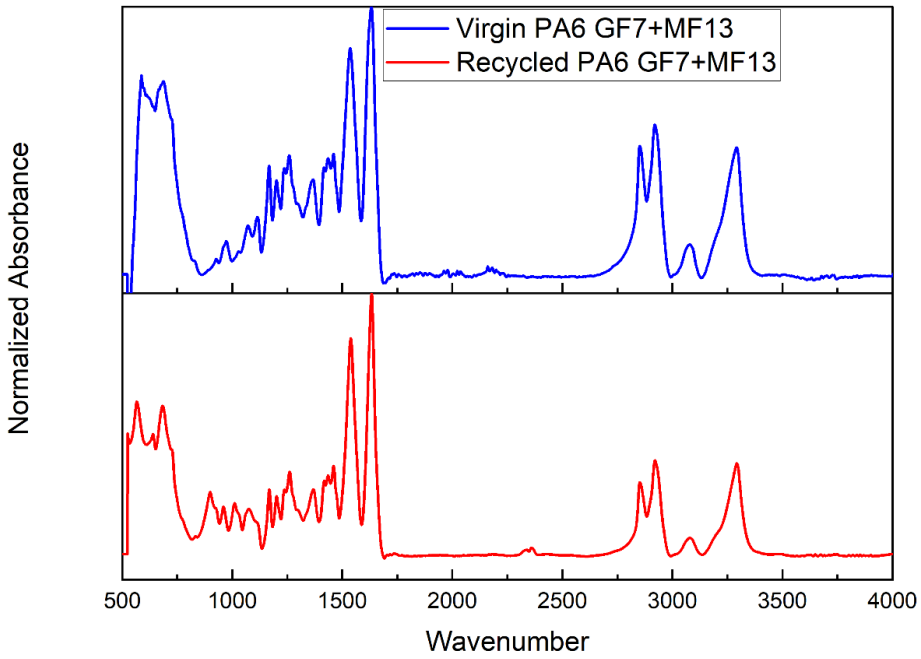


Figure 4.5 - FTIR spectra of injection molded virgin PA6+GF7+MF13 pellets and injection molded recycled PA6+GF7+MF13 granules.

Thermal Behavior: Differential Scanning Calorimetry (DSC)

To further visualize thermal transitions and degradation behavior across all materials, differential scanning calorimetry (DSC) thermograms were plotted for both virgin and end-of-life (EOL) samples under first and second heating cycles (**Figures 4.6 and 4.7**). In the first heat cycle (**Figure 4.6**), the virgin PP sample shows a sharp, well-defined melting peak near 165 °C, whereas the EOL PP sample displays a broader, less pronounced peak, indicative of thermal history effects such as oxidation or partial crystallinity loss. For PP-T10, the opposite trend was observed. EOL samples exhibited a more pronounced melting peak and a higher onset temperature relative to virgin samples, showing increased crystallinity. PP-T20 showed a moderate increase in melting enthalpy in EOL samples, with sharper peaks relative to virgin PP-T20, despite similar melting points. In PA6+GF7+MF13, both virgin and EOL samples displayed broader, high-temperature melting peaks (~220 °C), typical of semicrystalline PA. The EOL sample exhibited slightly enhanced peak intensity. The second heat DSC data, as seen in **Figure 4.7**, are critical for distinguishing intrinsic material properties from thermal history effects, as they eliminate reprocessing variables and isolate differences that are inherent to the base resin [58]. Crystallinity trends that persist in the second heat, for PP the crystallinity remained significantly lower in the EOL sample during both heat cycles and PP-T10 retained higher crystallinity across both cycles, suggests that these differences are not due to molding or processing history, but are intrinsic to the base material possibly caused by differences in tacticity or molecular weight, as discussed in Combined DSC–TGA Thermal and Crystallinity Trends.

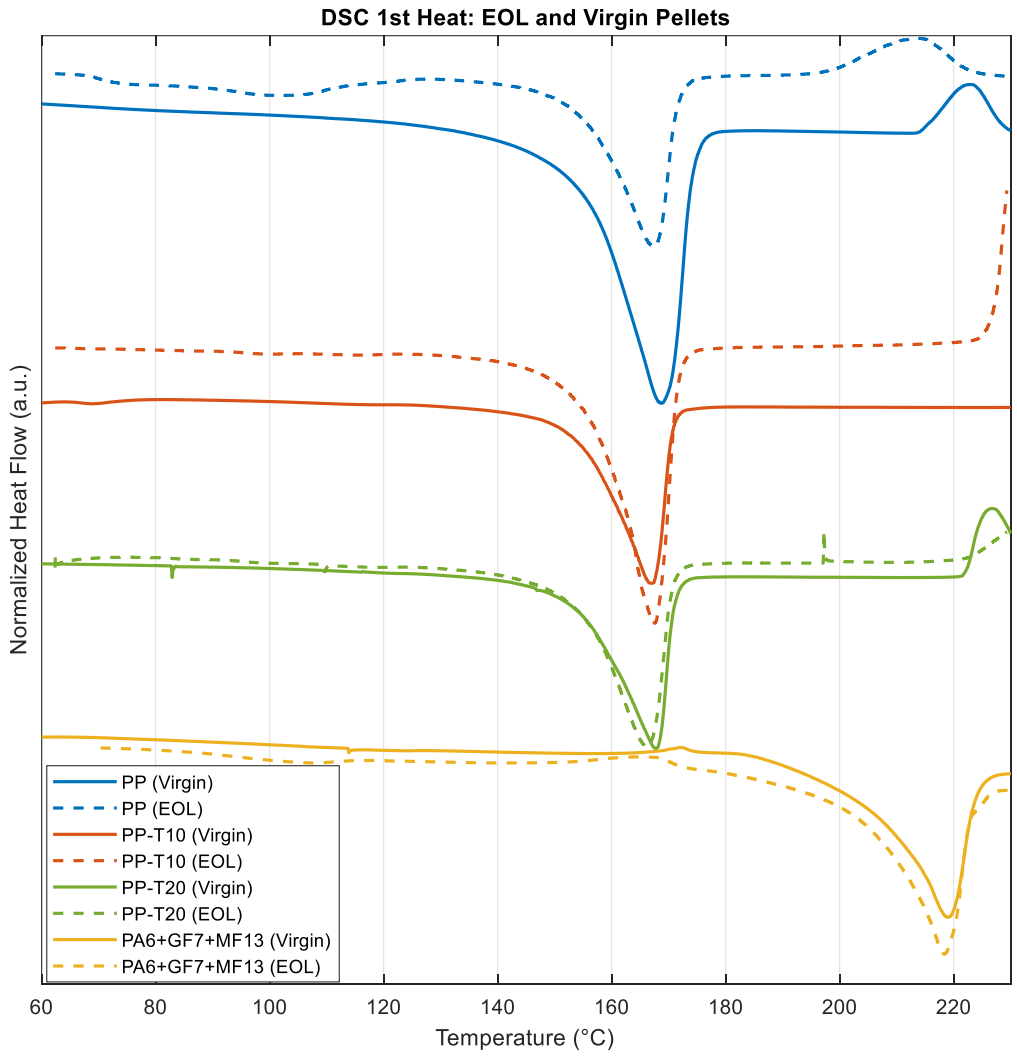


Figure 4.6 - DSC thermograms comparing virgin pellets and end-of-life (EOL) samples for all four material formulations from first heat cycle

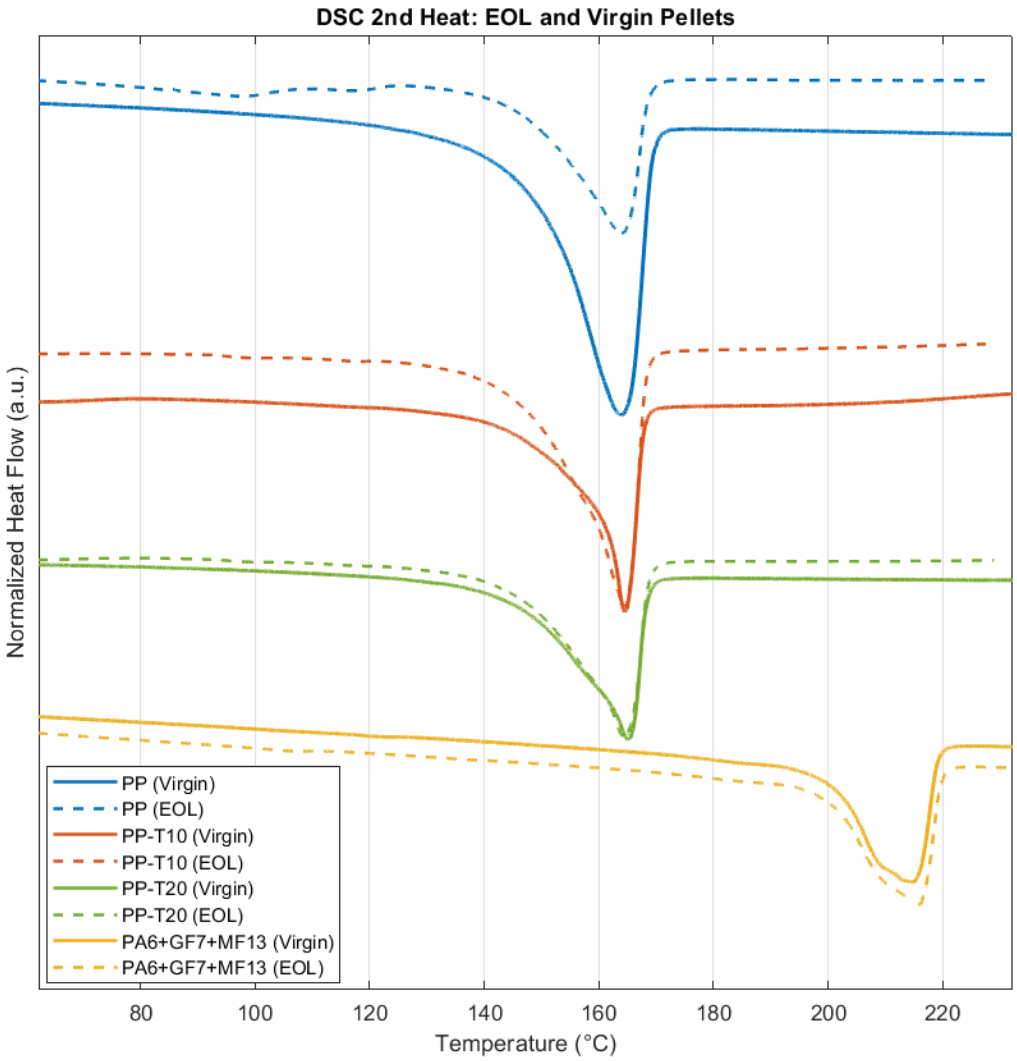


Figure 4.7 - DSC thermograms comparing virgin pellets and end-of-life (EOL) samples for all four material formulations from second heat cycle

Thermal Degradation: Thermogravimetric Analysis (TGA)

To further understand decomposition behavior and filler retention, thermogravimetric analysis (TGA) was performed on both virgin pellets and end-of-life (EOL) materials seen in **Figure 4.8** and quantified in **Table 4.1**. TGA tracks the percentage of mass lost as temperature increases, enabling quantification of residual mass at 600 °C.

The neat PP sample exhibited a increase in residual mass at 600 °C from $0.52 \pm 0.36\%$ in the virgin sample to $2.55 \pm 0.05\%$ in the EOL counterpart, suggesting possible contamination or residue accumulation over the service life. Moreover, the onset of thermal degradation, defined by the temperature at 2% weight loss in this work, occurred at a lower temperature in the EOL PP sample (268.2 ± 9.3 °C) compared to the virgin material (281.5 ± 0.6 °C), indicating thermal or oxidative degradation during use. For PP-T10, both the residual mass (~10%) and degradation onset temperature (~319.4 °C) remained nearly identical between virgin and EOL samples, reflecting high thermal stability and consistent filler content. PP-T20, on the other hand, showed a reduction in residual mass from $25.65 \pm 0.05\%$ to $20.51 \pm 0.11\%$, possibly due to filler loss or differences in actual formulation. Additionally, its degradation onset temperature dropped by nearly 20 °C, further supporting the possibility of resin degradation or batch inconsistency. The PA6+GF7+MF13 formulation showed minimal differences between virgin and EOL states, with residual mass values of $20.15 \pm 0.27\%$ and $20.20 \pm 1.09\%$ respectively, and only a slight shift in degradation onset temperature (342.0 ± 12.7 °C vs. 336.8 ± 6.3 °C).

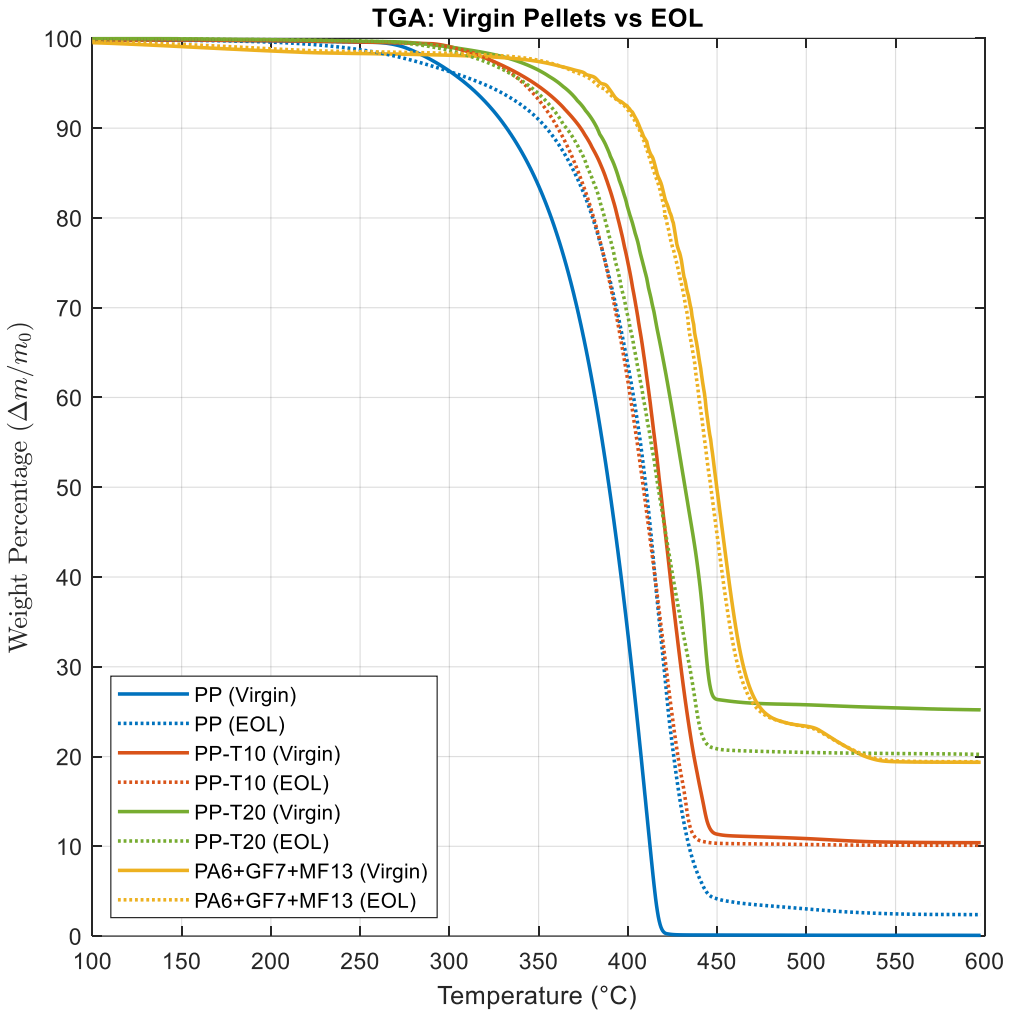


Figure 4.8 - Thermogravimetric analysis (TGA) curves showing mass loss profiles for virgin and recycled samples of all four material formulations. Virgin samples are shown as dashed lines; EOL samples as solid lines.

Table 4.1 - Residual mass at 600 °C (%) and temperature (°C) at 2% weight loss measured by TGA. Values are grouped by stage: Virgin Pellet, End-of-Life (EOL)

Material	**Virgin Pellet (% Mass)**	**EOL (% Mass)**	**Virgin Temp @ 2% Weight Loss (°C)**	**EOL Temp @ 2% Weight Loss (°C)**
PP	0.52 ± 0.36	2.55 ± 0.05	281.54 ± 0.63	268.19 ± 9.29
PP-T10	10.50 ± 0.11	10.14 ± 0.03	319.44 ± 1.69	319.43 ± 1.15
PP-T20	25.65 ± 0.05	20.51 ± 0.11	335.65 ± 7.62	316.33 ± 3.86
PA6+GF7+MF13	20.15 ± 0.27	20.20 ± 1.09	342.02 ± 12.66	336.84 ± 6.25

In most cases, the recycled samples retained a higher residual mass at 600 °C, consistent with the presence of inorganic filler, additives, or oxidative byproducts. PP-T20 and PA6+GF7+MF13 showed the greatest differences between virgin and recycled samples, supporting earlier observations from TGA bar plots and reinforcing the impact of formulation on thermal degradation resistance.

Combined DSC–TGA Thermal and Crystallinity Trends

To integrate thermal transitions with degradation profiles, results from differential scanning calorimetry (DSC) and thermogravimetric analysis (TGA) were plotted together for each formulation. These plots help visualize trends in melting temperature, crystallinity, and residual mass at 600 °C across all processing stages. To clarify, virgin and recycled samples originate from different sources and should not be interpreted as the same material undergoing a recycling loop. For example, the virgin PP sample was obtained from LyondellBasell, while the recycled PP sample was derived from ELV parts. For PP (**Figure 4.9**), a reduction in crystallinity is observed when comparing the end-of-life (EOL) PP samples to the injection molded virgin pellets. The virgin PP, sourced from LyondellBasell, exhibited a crystallinity of 46%, while the EOL PP, derived from post-consumer ELV parts, showed a significantly lower crystallinity of 26%. This lower crystallinity remained consistent through the recycled granules and injection molded recycled samples, which exhibited values of 26% and 28%, respectively. A corresponding increase in residual mass at 600 °C is also observed: the virgin PP retained only 0.52%, while EOL and recycled PP samples retained 2.55% and 9.45%, respectively.

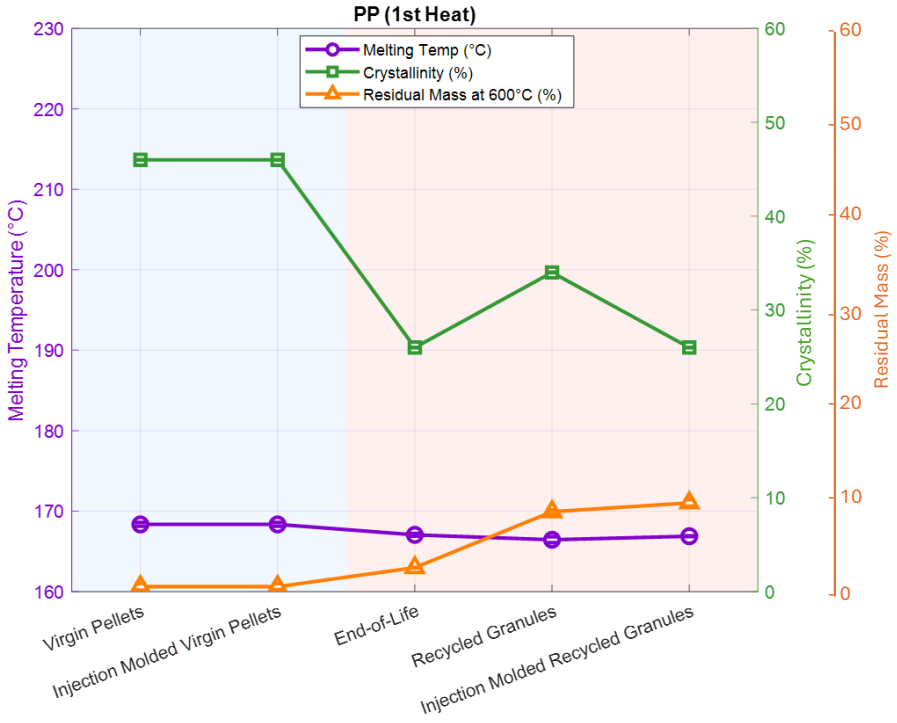


Figure 4.9 - Melting temperature, crystallinity, and residual mass at 600 °C for PP samples across all processing stages, based on DSC and TGA data from the first heating cycle.

This trend may indicate increasing contamination or variability in local filler content across post-use stages, potentially due to inconsistencies during original manufacturing or variability in the material distribution throughout the molded part that stemmed from its original processing conditions. These findings indicate that the observed differences in crystallinity are likely due to inherent differences in resin chemistry, such as tacticity or molecular weight, between the virgin and recycled PP samples, rather than degradation or reprocessing effects. In addition to, this trend is now further supported by FTIR data, which shows a unique peak near 1000 cm^{-1} in the recycled PP but not in the virgin material. This may indicate unsaturated chain ends, presence of an additive containing C-O bonds, or a change in stereoregularity. The virgin PP from LyondellBasell is possibly more isotactic in structure, whereas the ELV-derived PP may be more atactic [59]. Atactic PP would likely have reduced crystallinity due to its irregular chain packing, which could account for the consistently lower crystallinity values observed across EOL and recycled samples. It could also be that the presence of an additive is preventing crystallization in the EOL samples.

For PP-T10 (**Figure 4.10**), an increase in crystallinity is observed in the recycled and post-use materials compared to the separately sourced virgin PP-T10. The virgin PP-T10 sample exhibited a crystallinity of an average of 27% ± 0.00, while the EOL sample reached 41%± 0.01, and the recycled granules and injection molded recycled samples measured an average of 44% ± 0.02 and 40% ± 0.02, respectively. Since no significant changes in FTIR spectra or TGA residual mass were observed between the virgin and recycled PP-T10 samples, the increase in crystallinity is unlikely to be driven by

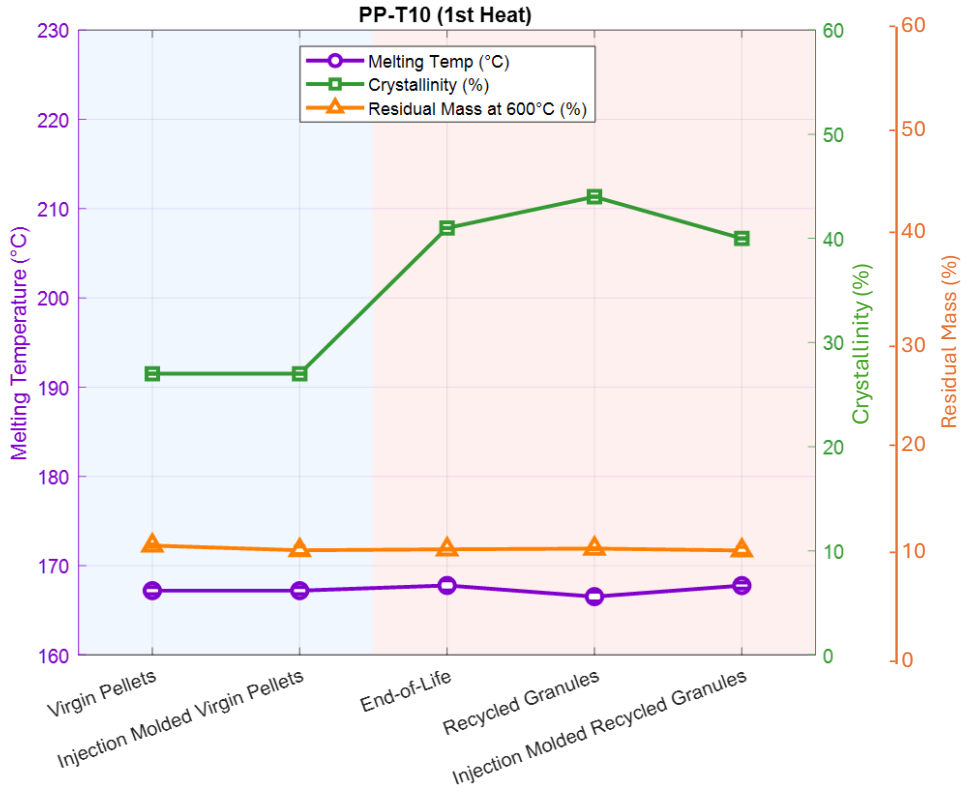


Figure 4.10 - Melting temperature, crystallinity, and residual mass at 600 °C for PP-T10 samples across all processing stages, based on first heat thermal analysis.

chemical additives or filler content. A likely explanation is a difference in molecular weight between the original and recycled PP-T10 resins. While molecular weight was not directly measured in this study, these findings suggest that subtle resin formulation differences may be driving the crystallinity increase in the post-use PP-T10 samples.

For PP-T20 (**Figure 4.11**), an increase in crystallinity is observed in the EOL and recycled samples compared to the virgin PP-T20, which was supplied by LyondellBasell. The virgin sample showed an average crystallinity of 30%± 0.01, while the EOL sample reached 35%± 0.01, and the recycled granules and injection molded recycled samples measured 34%± 0.01 and 38± 0.01%, respectively. These increases suggest differences in the resin or formulation between the automotive-sourced material and the model virgin material. At the same time, TGA analysis revealed a decreased residual mass at 600 °C in the recycled PP-T20 samples. The virgin material retained an average of 25.23%± 0.11, while the recycled granules and injection molded recycled samples retained an average of 20.48%± 0.08 and 20.45% ± 0.30, respectively. Since virgin PP-T20 was labeled as containing 20% filler but exhibited a higher than expected residual weight at 600 °C, this difference suggests the actual filler content may have exceeded the label claim. These differences in filler content could explain the observed changes in crystallinity and thermal response.

For PA6+GF7+MF13 (**Figure 4.12**), a slight increase in crystallinity is observed in the EOL sample (31% ± 0.01) compared to the virgin formulation from LyondellBasell (27% ± 0.01%), with a more pronounced jump seen in the shredded granules (45% ± 0.01).

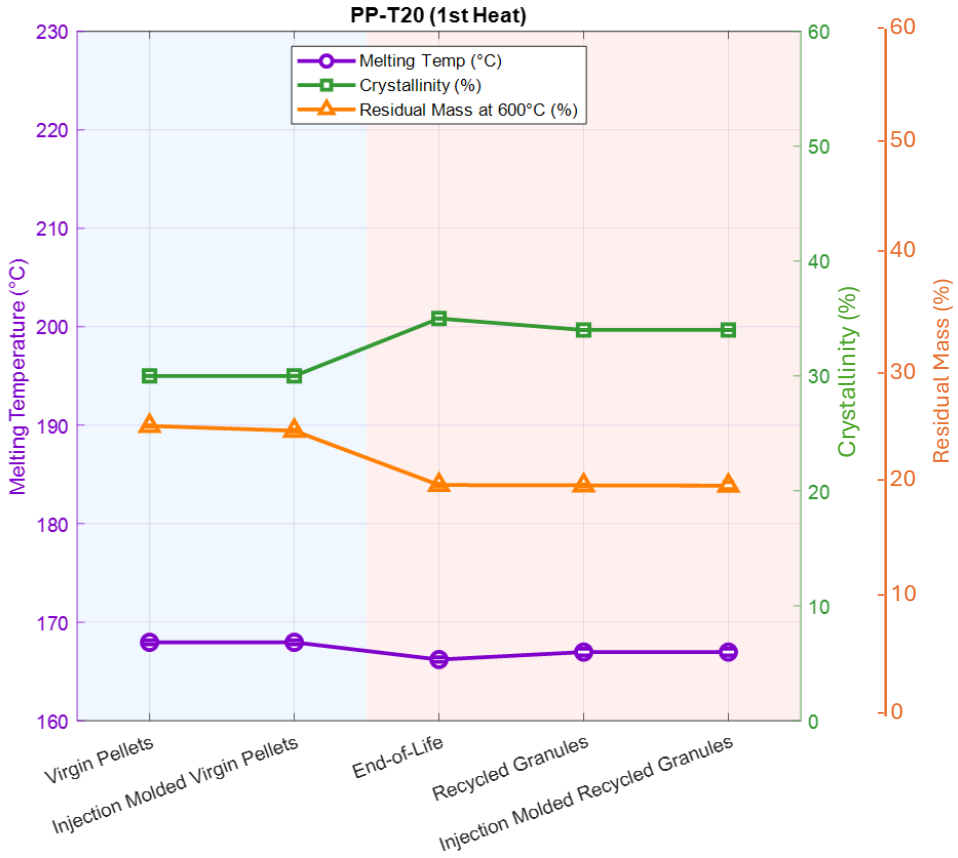


Figure 4.11 - Melting temperature, crystallinity, and residual mass at 600 °C for PP-T20 samples across all processing stages, derived from first heat DSC and TGA measurements.

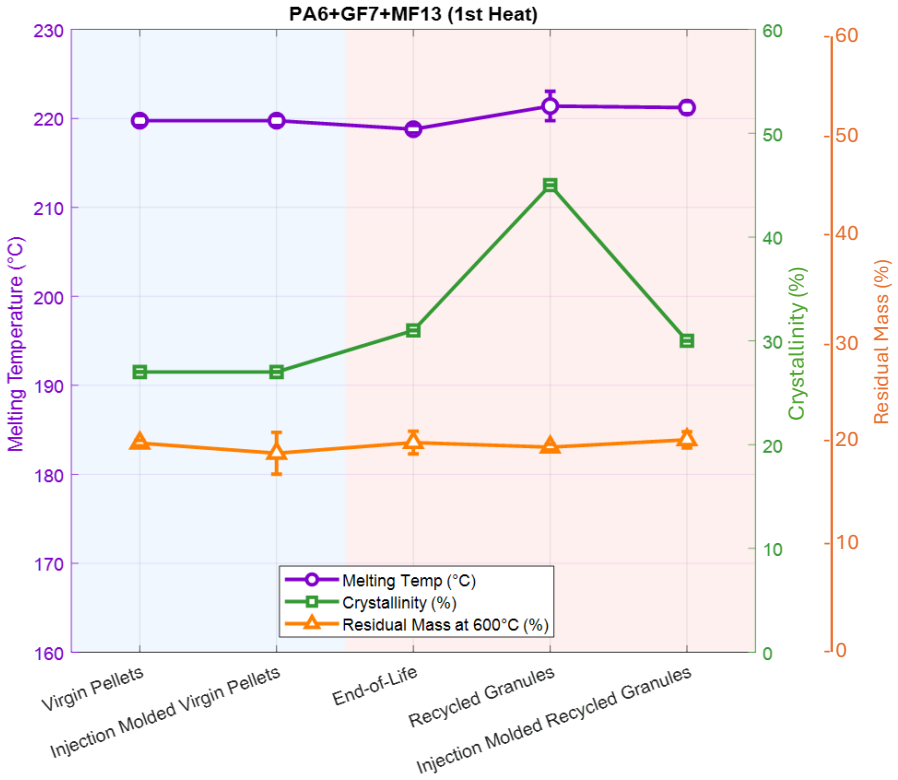


Figure 4.12 - Melting temperature, crystallinity, and residual mass at 600 °C for PA6+GF7+MF13 samples across all processing stages, as measured in the first heating cycle of DSC and TGA.

The virgin sample was supplied as a model formulation, while the EOL and recycled samples were recovered from actual automotive components.

The slight increase in crystallinity in this set could be due to an additive present in such low concentration that it is not detectable relative to the polymer matrix. It could also result from changes in molecular weight between the virgin and recovered materials, differences not yet quantified in this analysis. Despite these variations, residual mass at 600 °C remains relatively stable across all processing stages, 20.15% ± 0.27 for the virgin, 20.20% ± 1.09 for EOL, 19.76% ± 0.28 for the shredded granules, and 20.47% ± 0.78 for the injection molded recycled sample, consistent with the expected thermal stability of the glass and mineral fillers in the PA6 blend.

Mechanical Performance

Mechanical performance was evaluated for injection molded samples produced from virgin model formulations and from disassembled ELV-derived materials. Each material's tensile behavior is discussed individually.

For neat PP (**Figure 4.13**), the largest drop in mechanical performance was observed. Young's modulus decreased from 2.07 GPa to 1.38 GPa (33%), while UTS fell by nearly 50% (from ~40 MPa to ~20 MPa). The reduction in stiffness may be linked to the lower crystallinity observed in the ELV-derived PP samples, which had 26–28% crystallinity compared to 46% in the virgin model PP. Previous research has shown that more crystalline polymers can have higher stiffnesses, but lower strength [60]. However, this could also be degradation brought on by the use-life of the vehicle where the PP

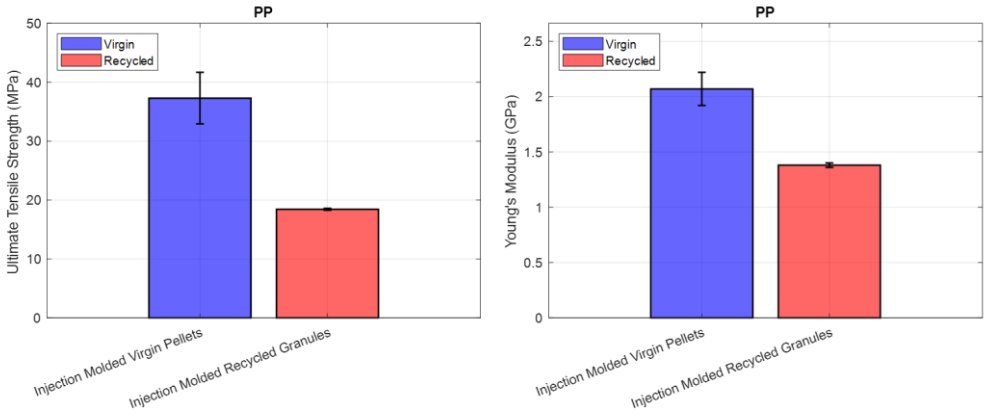


Figure 4.13 - Young's modulus and ultimate tensile strength of PP injection molded parts made from virgin pellets and recycled granules.

bumper fascia experienced thermal cycling and UV-ray exposure, which can induce molecular degradation of the polymer itself.

In PP-T10 samples (**Figure 4.14**), mechanical properties remained relatively consistent despite differences in origin between the injection molded virgin pellets and recycled granules. The virgin formulation, sourced from LyondellBasell, exhibited a UTS of 29.6 MPa and a Young's modulus of 1.8 GPa, while the recycled PP-T10, derived from end-of-life automotive components, measured 28.9 MPa in UTS and 2.15 GPa in modulus. These small differences suggest that the recycled material retains comparable stiffness and strength, possibly due to preserved filler content and similar resin chemistry. Although the recycled material exhibited higher crystallinity, mechanical properties remained comparable, suggesting that factors like molecular weight or stabilization may preserve mechanical performance.

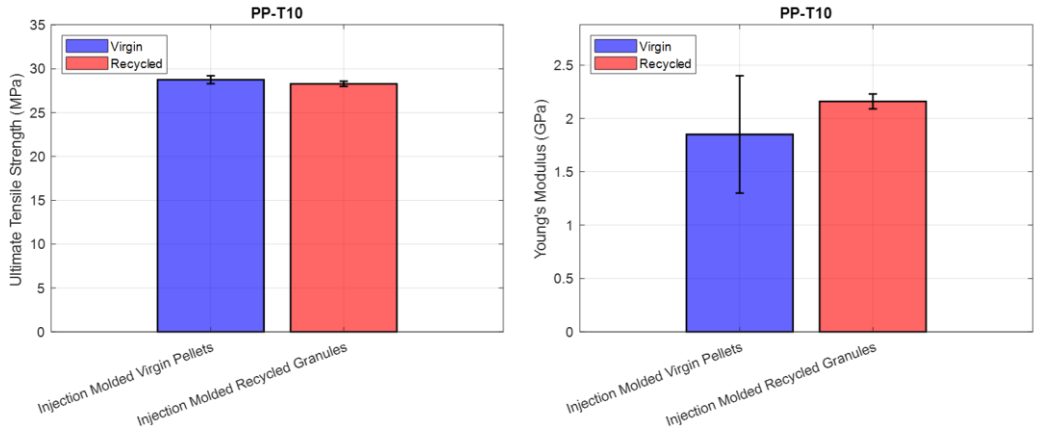


Figure 4.14 - Young's modulus and ultimate tensile strength of PP-T10 injection molded parts made from virgin pellets and recycled granules.

For PP-T20 (Figure 4.15), a 20.4% decrease in Young's modulus was observed (from 2.7 GPa to 2.15 GPa), along with a small reduction in UTS (from 28 MPa to 21 MPa). These reductions are likely influenced by lower filler content in the ELV-derived material, as supported by residual mass values from TGA. While crystallinity increased slightly, which may have improved stiffness, it may not have been enough to offset the loss of structural reinforcement due to fiber degradation or matrix weakening. As seen in this analysis, the reduction in modulus observed in PP-20 samples is most likely because the virgin samples contained additional filler within them on average as quantified by TGA. Talc is commonly used in PP composites to improve stiffness, dimensional stability, and heat deflection temperature by restricting polymer chain mobility through its plate-like morphology [60]. These benefits are evident in the virgin PP-T20 samples, which demonstrated higher modulus values and increased residual mass in TGA analysis, both indicative of higher filler content. However, talc can also increase ductility and impact resistance, which may explain the difference in UTS observed in the virgin PP-T20 samples [61].

Among all formulations, PA6+GF7+MF13 (**Figure 4.16**) demonstrated the highest stiffness with Young's modulus values ranging from 4.1 to 4.4 GPa. A slight reduction in modulus was observed in ELV-based recycled samples, but values remained within a high-performance range. In contrast to its modulus trend, UTS decreased from ~105 MPa to ~90 MPa (a ~15% drop), likely due to glass fiber breakage or fiber-matrix interface degradation during shredding and reprocessing [62]. It is possible that during the recycling process,

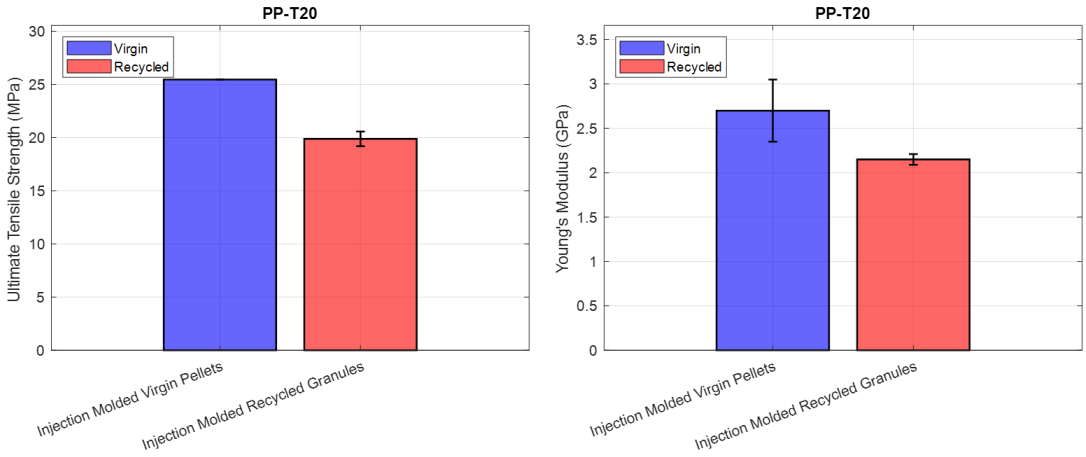


Figure 4.15 - Young's modulus and ultimate tensile strength of PP-T20 injection molded parts made from virgin pellets and recycled granules.

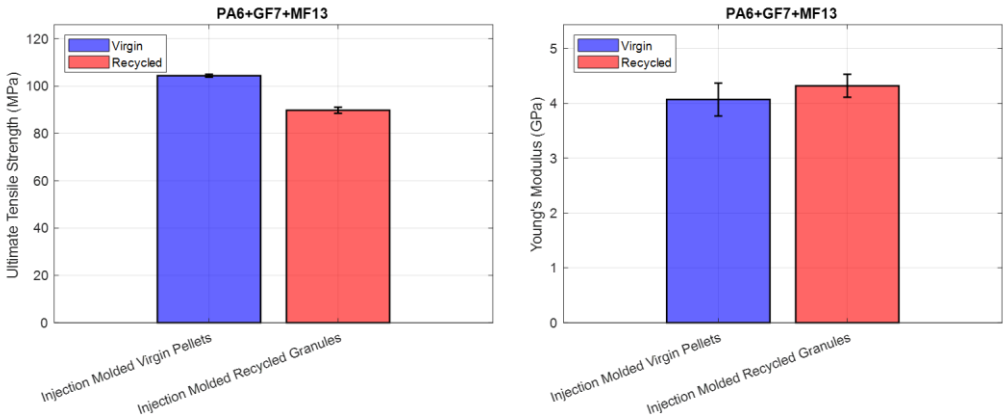


Figure 4.16 - Young's modulus and ultimate tensile strength of PA6-GF7-MF13 injection molded parts made from virgin pellets and recycled granules.

glass fiber breakage in the PA6-GF7-MF13 samples drove the reduction in strength observed in the recycled samples.

Figure 4.17 displays the average heat deflection temperature (HDT) values for injection molded parts made from both virgin pellets (blue) and recycled granules (red) across all four material formulations. Although reductions in mechanical strength and stiffness were observed in some recycled materials, HDT values did not significantly change between virgin and recycled samples. This indicates that thermomechanical stability is retained despite molecular or structural changes introduced through end-of-life conditions and reprocessing. Such stability is especially relevant for parts that must maintain shape and function under elevated temperatures.

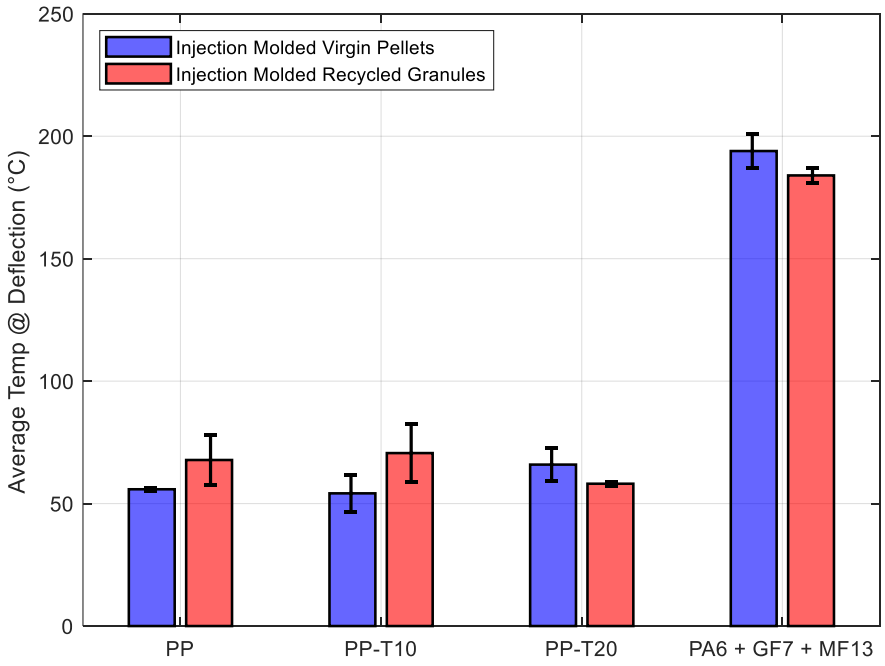


Figure 4.17 - Heat deflection temperature (°C) results from injected molded parts made from both virgin pellets and recycled granulates.

The HDT results reinforce a key insight from this study: while mechanical recycling of ELV plastics can result in materials with altered crystallinity, density, and mechanical strength compared to model formulations, the core ability of these materials to meet temperature-related functional requirements remains intact. These findings are particularly important in the context of automotive applications, where dimensional stability under heat is critical for components used under the hood or within the cabin. The preservation of HDT values across all tested material formulations suggests that disassembled and mechanically recycled plastics, especially those reinforced with mineral or glass fillers, retain sufficient performance for use in secondary automotive applications.

CHAPTER FIVE

CONCLUSIONS AND RECOMMENDATIONS

This study demonstrates the value of mechanically recycling unpainted thermoplastic parts recovered from ELVs and reintroducing them into the automotive value chain. Across the four tested material types: PP, PP-T10, PP-T20, and PA6+GF7+MF13, recycled samples exhibited modest differences in density, crystallinity, and filler content but largely retained mechanical properties within a performance range suitable for secondary use. Specifically, filled PP and glass/mineral-filled PA samples showed particularly promising retention of modulus and HDT, supporting their potential reuse in under-the-hood or structural applications. Variability in the resins (including additives, fillers, and molecular structure) could have contributed to the differences measured in the samples. The findings suggest that while part disassembly, combined with direct granule-based reprocessing, can offer a practical and scalable approach to improving ELV plastic recovery rates without significant loss of material performance, there is more work needed to identify materials at EOL. Relying on labels on parts alone does not account for variability in resin chemistry, as observed in this work. Variability in additives, resin chemistries, and molecular weights could be contributing to changes in functional performance observed. However, these results suggest that there is residual value in performance of ELV plastics, though the specifications will need to be measured and quantified. This work contributes to growing evidence that mechanical recycling of targeted plastic streams, especially when paired with material-specific disassembly, can support broader goals of automotive circularity, cost reduction, and landfill diversion.

To advance this work beyond a feasibility study, future research should prioritize full life-cycle traceability of plastic components. Ideally, partnerships with OEMs, resin suppliers, and molders would enable a controlled cradle-to-grave study where specific materials are followed from manufacturing through their in-vehicle lifespan, then recovered and recycled for direct performance comparison. This level of traceability would help isolate the effects of service-life exposure on material degradation and enable side-by-side evaluation of virgin and recycled components molded from the same source.

Scaling the process is another critical next step. While this study demonstrated consistent injection molding performance from small granulate batches, industrial viability depends on the ability to process large volumes. Future efforts should include disassembly and recycling of several hundred kilograms, preferably an entire Gaylord box, of a single part type, such as bumpers or engine covers. This would support meaningful mechanical property distributions, validate part consistency, and reveal processing challenges not visible at lab scale.

In addition to scaling volume, it will be important to source material from multiple scrapyard facilities across regions and dismantling methods. The components in this study came from a single location, limiting insight into how site-to-site variability affects recyclability. Future work should capture a wider range of dismantling conditions, storage durations, and climate exposure to evaluate how those factors influence material quality and performance.

Furthermore, the economic and environmental implications of this recovery method must be quantified to justify its implementation at scale. A detailed techno-

economic analysis should include labor requirements for part removal, shredder operation, drying energy, and molding throughput to calculate the true cost per pound of recycled material. Parallel to this, a cradle-to-gate life cycle assessment [LCA] is recommended to quantify the carbon footprint, energy savings, and landfill diversion achieved through this approach compared to traditional disposal and virgin resin production. Together, these metrics will be key to aligning sustainability targets with commercial feasibility.

To further bridge the gap between technical feasibility and implementation, future work should also prioritize application-specific testing of recycled materials. While tensile bars provide valuable baseline metrics, real-world parts, such as brackets, clips, or covers, may experience different loading, flow, and cooling conditions during molding. Validating recycled performance in these part geometries will better inform end-use decisions. Additionally, consistent and clear material labeling from OEMs will be critical to enabling scalable recovery. Standardized part markings with detailed resin and filler content can significantly improve traceability and reduce the need for time-intensive material identification at disassembly.

LIST OF REFERENCES

1. OICA, *WORLD MOTOR VEHICLE PRODUCTION BY COUNTRY/REGION AND TYPE* 2025.
2. ACEA, *Economic and Market Report Global and EU auto industry: Full year 2023*. 2023.
3. Energy, U.S.D.o., *Vehicle Registration Counts by State.* 2023.
4. Book, K.B. *Kelley Blue Book Report: Average New-Vehicle Prices Climb Higher For Fourth Consecutive Month, Flirt with All-Time High*

2025 [cited 2025 May 3].

5. Proost, S. and K. Van Dender, *Energy and environment challenges in the transport sector.* Economics of Transportation, 2012. **1**(1-2): p. 77-87.
6. Rose-Glowacki, H., *Chemistry and Automobiles Driving the Future*. 2024.
7. Zhu, G., et al., *Energy absorption of metal, composite and metal/composite hybrid structures under oblique crushing loading.* International Journal of Mechanical Sciences, 2018. **135**: p. 458-483.
8. Korey, M., et al., *Durable Automotive Plastics Circularity Report*. 2024.
9. EuRIC, *EuRIC Call for Recycled Plastic Contentin Cars.* 2020.
10. Exchange, T.P. *Resin Markets*. 2025 [cited 2025 May 3]; Available from: https://www.theplasticsexchange.com/.
11. Hamza, A., et al., *Revolutionizing Automotive Design: The Impact of Additive Manufacturing.* Vehicles, 2025. **7**(1): p. 24.

12. Vijayan, S.K., V. Sahajwalla, and S. Bhattacharya, *Insights into the options of energy and metal recovery from automotive shredder residue: A review.* Resources, Conservation & Recycling Advances, 2022. **15**: p. 200097.

13. Held, M., et al., *Lifespans of passenger cars in Europe: empirical modelling of fleet turnover dynamics.* Eur Transp Res Rev, 2021. **13**(1): p. 9.

14. EPRB, *Robust recycled content for plastics in vehicles essential to drive plastic recycling in Europe.* 2024.

15. Alyssa Knowlton, S.B., Ph.D., and Bryan Staley, Ph.D., P.E., *ANALYSIS OF MSW LANDFILL TIPPING FEES - 2023*. 2023.

16. Rose-Glowacki, H., *Chemistry and Automobiles Driving the Future*

2024.

17. Maury, T., et al., *Towards recycled plastic content targets in new passenger cars and light commercial vehicles – Technical proposals and analysis of impacts in the context of the review of the ELV Directive*. 2023, Publications Office of the European Union.

18. Council, E.P.a., *Directive 2000/53/EC of the European Parliament and of the Council of 18 September 2000 on end-of life vehicles*. 2000, Official Journal of the European Communities.

19. Recovery, C.D.o.R.R.a., *Plastic Pollution Prevention and Packaging Producer Responsibility Act: Implementation Report to the Legislature*. 2025: Sacramento, CA.

20. Sakai, S.-i., Y. Noma, and A. Kida, *End-of-life vehicle recycling and automobile shredder residue management in Japan.* Journal of Material Cycles and Waste Management, 2007. **9**(2): p. 151-158.

21. Howard, K.L., *BIORECYCLING*

OF PLASTICS. 2022.

22. Hasan, M., et al., *Energy recovery from municipal solid waste using pyrolysis technology: A review on current status and developments.* Renewable and Sustainable Energy Reviews, 2021. **145**: p. 111073.

23. de Mello Soares, C.T., et al., *Recycling of multi-material multilayer plastic packaging: Current trends and future scenarios.* Resources, conservation and recycling, 2022. **176**: p. 105905.

24. ExxonMobil. *ExxonMobil to Expand Advanced Recycling Capacity*. 2024 [cited 2025 May 3]; Available from: https://investor.exxonmobil.com/company-information/press-releases/detail/1176/exxonmobil-to-expand-advanced-recycling-capacity.

25. Eastman. *Tennessee Site – Circularity*. 2024 [cited 2025 May 3]; Available from: https://www.eastman.com/en/sustainability/environmental/circularity/site-locations/tennessee-site

26. Umdagas, L.B., et al., *Towards Sustainable Pet Recycling: Insights into Neutral Hydrolysis and Process Optimisation.* Available at SSRN 5061904.

27. Company, E.C. *Eastman to Invest Up to $1 Billion to Accelerate Circular Economy*. 2022 [cited 2025 May 3]; Available from: https://www.eastman.com/en/media-center/news-stories/2022/eastman-invest-accelerate-circular-economy.

28. Hou, Q., et al., *Upcycling and catalytic degradation of plastic wastes.* Cell Reports Physical Science, 2021. **2**(8).

29. Han, J., et al., *A systematic review of PET circularity technologies and management strategies: Challenges and future directions.* Resources, Conservation and Recycling, 2025. **219**: p. 108280.

30. Bergeson, A.R., A.J. Silvera, and H.S. Alper, *Bottlenecks in biobased approaches to plastic degradation.* Nature Communications, 2024. **15**(1): p. 4715.

31. Jody, B., et al., *End-of-life vehicle recycling: state of the art of resource recovery from shredder residue.* 2011.

32. Martín, A.J., et al., *Catalytic processing of plastic waste on the rise.* Chem, 2021. **7**(6): p. 1487-1533.

33. Sohrab Haghighi Mood, G.Y., Manuel GarciaPerez, *Evaluation of Emerging Plastics Recycling Technologies and management Strategies* 2023.

34. Munoz Meneses, R.A., et al., *Plastic recycling and their use as raw material for the synthesis of carbonaceous materials.* Heliyon, 2022. **8**(3): p. e09028.

35. Saleem, J., et al., *Assessing the environmental footprint of recycled plastic pellets: A life-cycle assessment perspective.* Environmental Technology & Innovation, 2023. **32**.

36. Maury, T., Tazi, N., Torres de Matos, C., Nessi, S., Antonopoulos, I., and E. Pierri, Baldassarre, B., Garbarino, E., Gaudillat, P., Mathieux, F., *Towards recycled plastic content targets in new passenger cars and light commercial vehicles*. 2023.

37. Arena, U. and F. Ardolino, *Technical and environmental performances of alternative treatments for challenging plastics waste.* Resources, Conservation and Recycling, 2022. **183**.

38. Jiao, H., et al., *A critical review on plastic waste life cycle assessment and management: Challenges, research gaps, and future perspectives.* Ecotoxicology and Environmental Safety, 2024. **271**: p. 115942.

39. Franklin Associates, A.D.o. and E.R.G. (ERG), *LIFE CYCLE IMPACTS FOR POSTCONSUMERRECYCLED RESINS: PET, HDPE, AND PP*. 2018.

40. Company, F.M. *Ford Bronco Sport Features First-Ever Parts Made of 100% Recycled Ocean Plastic*. 2021 [cited 2025 May 3]; Available from: https://media.ford.com/content/fordmedia/fna/us/en/news/2021/12/08/ford-bronco-sport-recycled-ocean-plastic.html

41. Bowden-Eyre, J. *Jaguar Land Rover Will Use Plastic Waste in Next-Generation Sustainable Luxury Interiors*. 2020 [cited 2025 May 3]; Available from: https://www.jlr.com/news/2020/09/jaguar-land-rover-will-use-plastic-waste-next-generation-sustainable-luxury-interiors.

42. Seidel, C. *BMW i Ventures invests in high-performance composites made from natural fibres.* 2022 [cited 2025 June 3]; Available from: https://www.press.bmwgroup.com/global/article/detail/T0377293EN/bmw-i-ventures-invests-in-high-performance-composites-made-from-natural-fibres?language=en.

43. Datz, R. *The all-electric Volvo EX30 small SUV is designed to have the lowest carbon footprint of any Volvo car to date*. 2023 [cited 2025 May 3]; Available from: https://www.media.volvocars.com/global/en-gb/media/pressreleases/312698/the-all-electric-volvo-ex30-small-suv-is-designed-to-have-the-lowest-carbon-footprint-of-any-volvo-c.

44. Co, H.R.D. *Honda and Idemitsu Kosan Begin Joint Demonstration Testing of Closed-loop Recycling of Plastics from End-of-Life Vehicles*. 2024 [cited 2025 May 3]; Available from: https://global.honda/en/topics/2024/c_2024-03-28eng.html.

45. Bisch, J. *LyondellBasell and Audi create first automotive plastic parts from mixed automotive plastic waste*. 2022 [cited 2025 May 3]; Available from: https://www.lyondellbasell.com/en/news-events/products--technology-news/lyondellbasell-and-audi-create-first-automotive-plastic-parts-from-mixed-automotive-plastic-waste/.

46. INDUTRY, P.I., *Ultra-Poly Corporation Recycles Plastic Car Bumpers with High Degree of Purity*. 2015.

47. Harler, C. *Recovering and recycling plastics from ASR is challenging, though some companies have found success.*

. 2015 [cited 2025 June 3]; Available from: https://www.recyclingtoday.com/article/rt0715-plastics-from-asr/#:~:text=Recovering%20and%20recycling%20plastics%20from,some%20companies%20have%20found%20success.&text=Automotive%20shredder%20residue%2C%20or%20ASR,material%20is%20plastics%E2%80%94valuable%20plastics.

48. Polymers, M. *Experience. Technology. Capabilities.* 2024 [cited 2025 June 3]; Available from: https://mbapolymers.com/.

49. Rezaei Abadchi, M. and A. Jalali-Arani, *Crystallization and melting behavior of polypropylene (PP) in (vulcanized nanoscale polybutadiene rubber powder/PP) polymer-nanocomposites.* Thermochimica Acta, 2015. **617**: p. 120-128.

50. Millot, C., et al., *Assessment of polyamide-6 crystallinity by DSC.* Journal of Thermal Analysis and Calorimetry, 2015. **122**(1): p. 307-314.

51. Korey, M., et al., *Recycling polymer composite granulate/regrind using big area additive manufacturing.* Composites Part B: Engineering, 2023. **256**: p. 110652.

52. Andoni, A., *A flat model approach to Ziegler-Natta olefin polymerization catalysts.* International Journal of Nonlinear Sciences and Numerical Simulation - INT J NONLINEAR SCI NUMER SIM, 2009.

53. Abo, H. *Distinction of Polyethylene and Polypropylene*

by Infrared Spectrum. 2024.

54. Andoni, A., *A flat model approach to Ziegler-Natta olefin polymerization catalysts.* 2009.

55. Luongo, J.P., *Infrared study of polypropylene.* Journal of Applied Polymer Science, 1960. **3**(9): p. 302-309.

56. Vaughan, A.S. and D.C. Bassett, *12 - Crystallization and Morphology*, in *Comprehensive Polymer Science and Supplements*, G. Allen and J.C. Bevington, Editors. 1989, Pergamon: Amsterdam. p. 415-457.

57. Kherroub, D., et al., *Synthesis of Polyamide-6/Montmorillonite Nanocomposites by Direct In-situ Polymerization Catalysed by Exchanged Clay.* Oriental Journal of Chemistry, 2014. **29**: p. 1429-1436.

58. Menczel, J.D., et al., *Differential scanning calorimetry (DSC).* Thermal analysis of polymers: Fundamentals and applications, 2009: p. 7-239.

59. DeMseuse, M.T., *4 - Polyolefins used in biaxial stretched films*, in *Biaxial Stretching of Film*, M.T. DeMeuse, Editor. 2011, Woodhead Publishing. p. 36-46.

60. Bakar, M.A., et al., *Mechanical, flow, and morphological properties of talc-and kaolin-filled polypropylene hybrid composites.* Journal of Applied Polymer Science, 2007. **104**(1): p. 434-441.

61. Fiorentino, B., et al., *Chemical modification routes of synthetic talc: Influence on its nucleating power and on its dispersion state.* Applied Clay Science, 2015. **109-110**: p. 107-118.

62. Diani, M. and M. Colledani, *Energy consumption assessment and modeling of a comminution process: the glass fibers reinforced composites case-study.* Procedia CIRP, 2020. **90**: p. 483-487.

APPENDIX

Table 5.1 - DSC results comparing virgin pellets with end-of-life (EOL) materials. Values reflect thermal properties during both the first and second heating cycles.

Sample	Melting Temp (1st Heat, °C)	Melting Temp (2nd Heat, °C)	Crystallinity (1st Heat, %)	Crystallinity (2nd Heat, %)
PP (Virgin Pellets)	168.35 ± 0.24	163.56 ± 0.20	46 ± 0.01	50 ± 0.00
PP (EOL)	167.05 ± 0.17	163.70 ± 0.36	26 ± 0.01	26 ± 0.01
PP-T10 (Virgin Pellets)	167.20 ± 0.40	164.80 ± 0.13	27 ± 0.00	30 ± 0.00
PP-T10 (EOL)	167.78 ± 0.56	164.30 ± 0.62	41 ± 0.01	48 ± 0.03
PP-T20 (Virgin Pellets)	167.95 ± 0.20	164.88 ± 0.21	30 ± 0.01	34 ± 0.01
PP-T20 (EOL)	166.20 ± 0.24	164.48 ± 0.21	35 ± 0.01	39 ± 0.03
PA6+GF7+MF13 (Virgin Pellets)	219.75 ± 0.56	215.39 ± 0.96	27 ± 0.01	27 ± 0.00
PA6+GF7+MF13 (EOL)	218.79 ± 0.42	216.15 ± 0.13	31 ± 0.02	29 ± 0.01

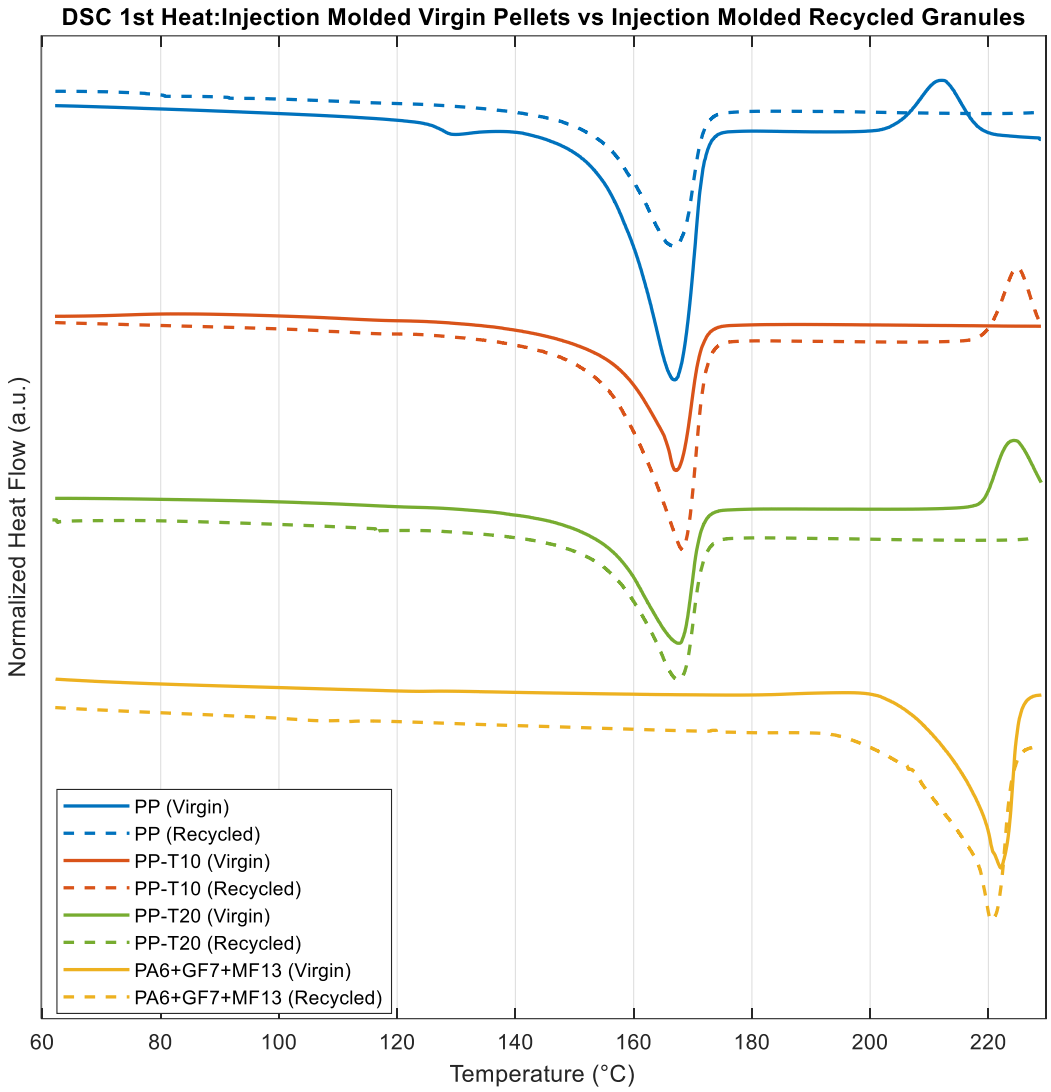


Figure 5.1 - DSC thermograms comparing injection molded virgin pellets and injection molded recycled granules samples for all four material formulations for first heat.

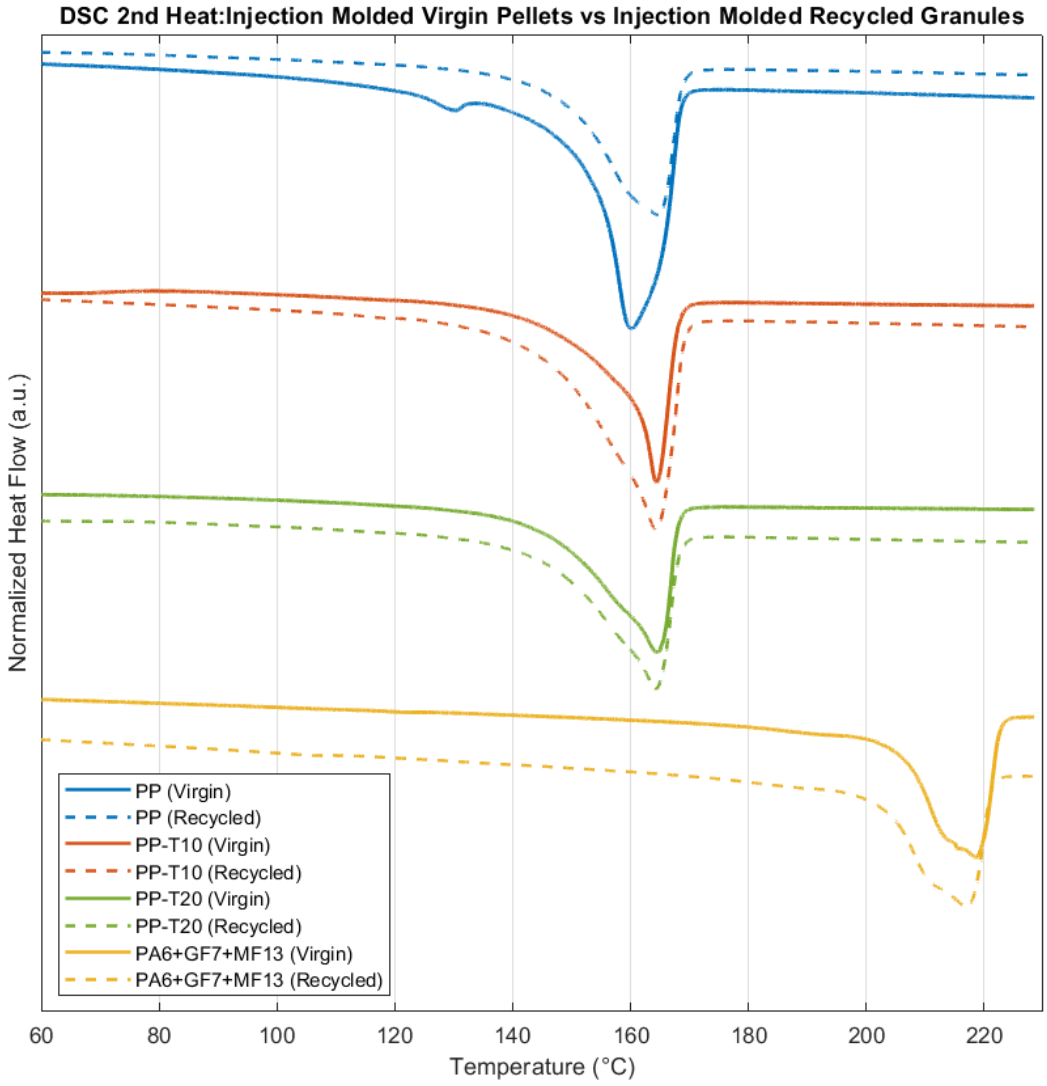


Figure 5.2 - DSC thermograms comparing injection molded virgin pellets and injection molded recycled granules samples for all four material formulations for second heat.

Table 5.2 - DSC results comparing injection molded virgin pellets and injection molded recycled granules. Values reflect thermal properties during both the first and second heating cycles.

Sample	Melting Temp (1st Heat, °C)	Melting Temp (2nd Heat, °C)	Crystallinity (1st Heat, %)	Crystallinity (2nd Heat, %)
PP (Injection Molded Virgin)	168.35 ± 0.24	163.56 ± 0.20	46 ± 0.01	50 ± 0.00
PP (Injection Molded Recycled)	166.88 ± 0.05	164.37 ± 0.36	26 ± 0.01	28 ± 0.01
PP-T10 (Injection Molded Virgin)	167.20 ± 0.40	164.80 ± 0.13	27 ± 0.00	30 ± 0.00
PP-T10 (Injection Molded Recycled)	167.77 ± 0.33	164.18 ± 0.05	40 ± 0.02	50 ± 0.45
PP-T20 (Injection Molded Virgin)	167.95 ± 0.20	164.88 ± 0.21	30 ± 0.01	34 ± 0.01
PP-T20 (Injection Molded Recycled)	166.96 ± 0.34	164.24 ± 0.05	34 ± 0.01	38 ± 0.01
PA6+GF7+MF13 (Injection Molded Virgin)	219.75 ± 0.56	215.39 ± 0.96	27 ± 0.01	27 ± 0.00
PA6+GF7+MF13 (Injection Molded Recycled)	221.22 ± 0.69	217.99 ± 1.87	30 ± 0.01	30 ± 0.01

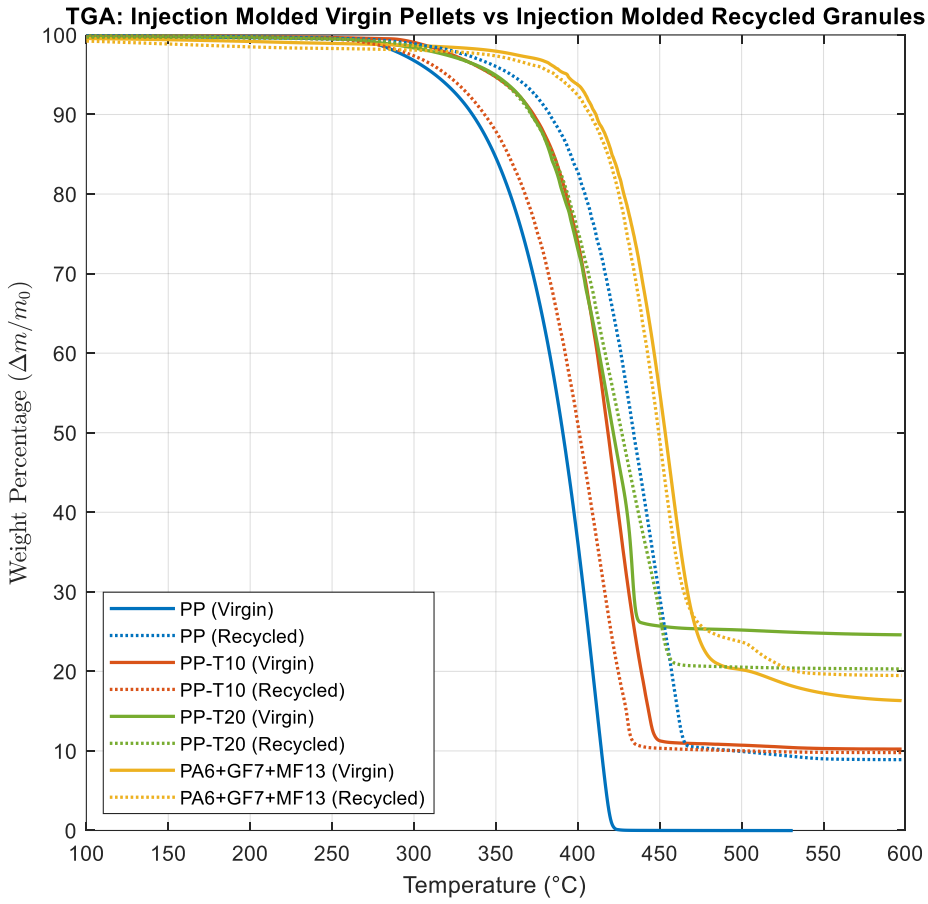


Figure 5.3 - Thermogravimetric analysis (TGA) curves showing mass loss profiles for injection molded virgin and recycled samples across all four material formulations. Virgin samples are shown as solid lines, recycled samples as dashed lines.

Table 5.3 - Residual mass at 600 °C (%) and temperature (°C) at 2% weight loss measured by TGA. Values are grouped by stage: Injection Molded Virgin Pellet, and Injection Molded Recycled Granule.

Material	Injection Molded Virgin Pellet (% Mass)	Injection Molded Recycled Granule (% Mass)	Virgin Temp @ 2% WL (°C)	Recycled Temp @ 2% WL (°C)
PP	0.52 ± 0.32	9.45 ± 0.34	277.95 ± 2.58	317.14 ± 8.93
PP-T10	10.05 ± 0.36	10.03 ± 0.32	314.64 ± 1.41	292.76 ± 2.74
PP-T20	25.23 ± 0.11	20.45 ± 0.30	313.96 ± 6.53	305.03 ± 5.01
PA6+GF7+MF13	19.17 ± 2.01	20.47 ± 0.78	353.18 ± 10.12	305.59 ± 2.78

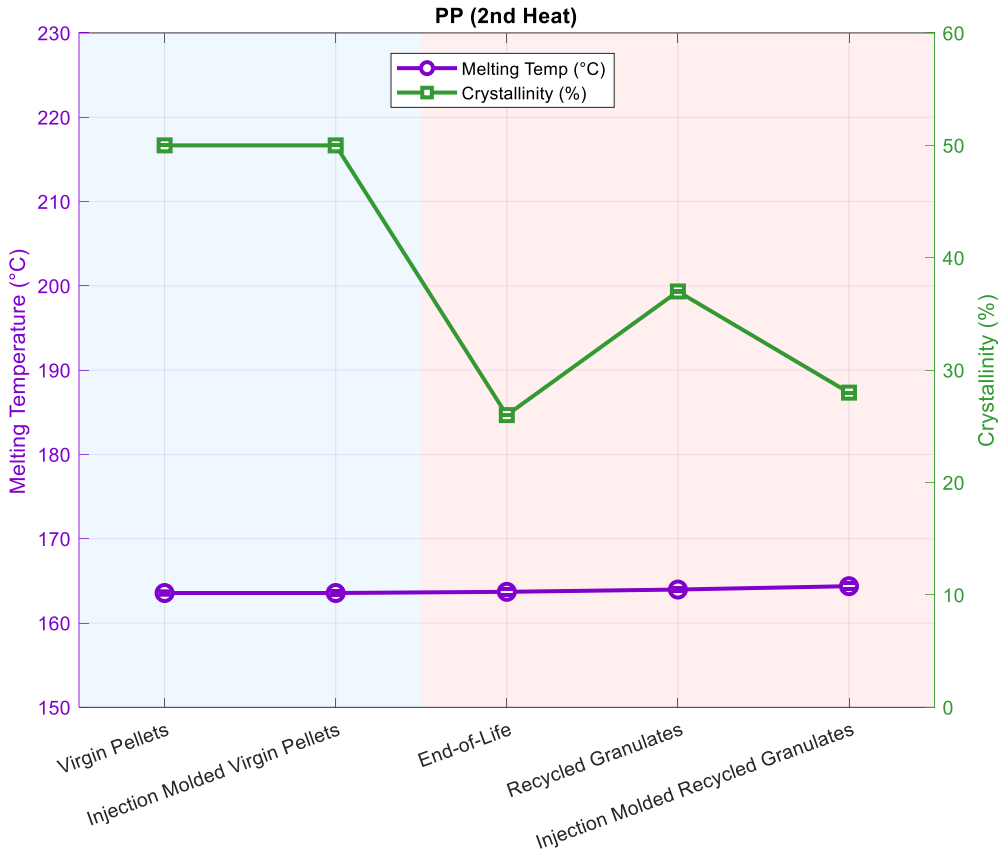


Figure 5.4 - Melting temperature and crystallinity for PP samples across all processing stages, based on second heat thermal analysis.

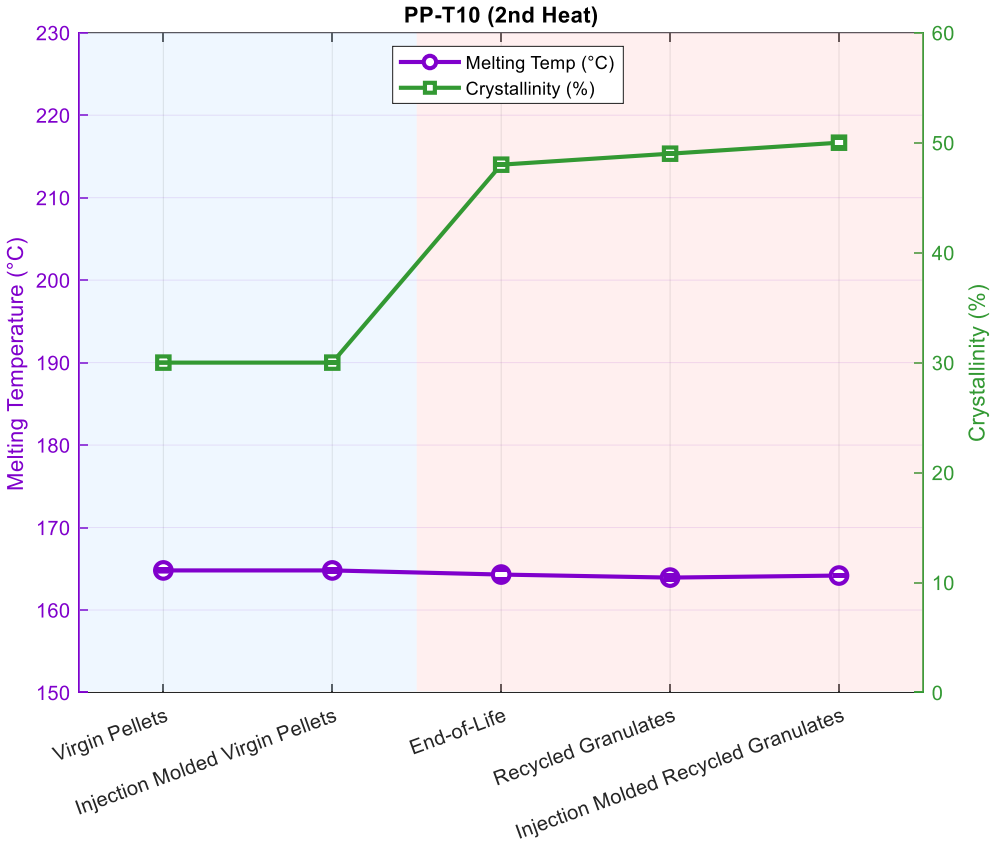


Figure 5.5 - Melting temperature and crystallinity for PP-T10 samples across all processing stages, based on second heat thermal analysis

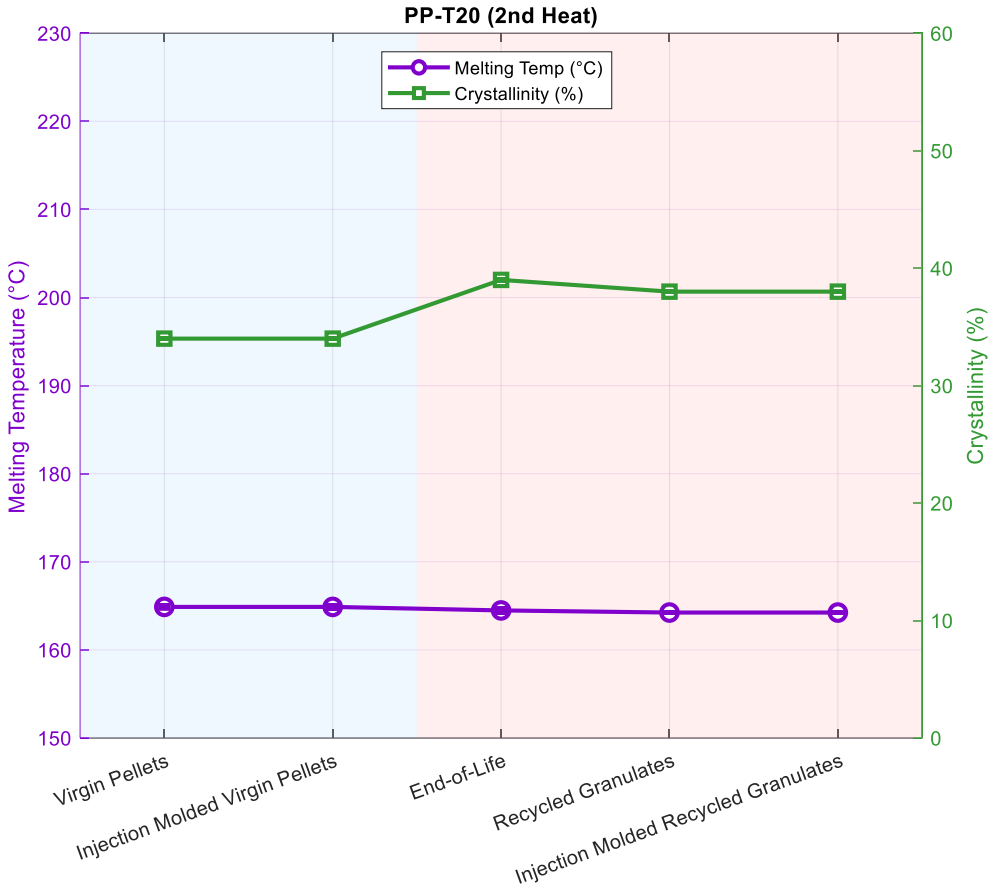


Figure 5.6 - Melting temperature and crystallinity for PP-T20 samples across all processing stages, based on second heat thermal analysis

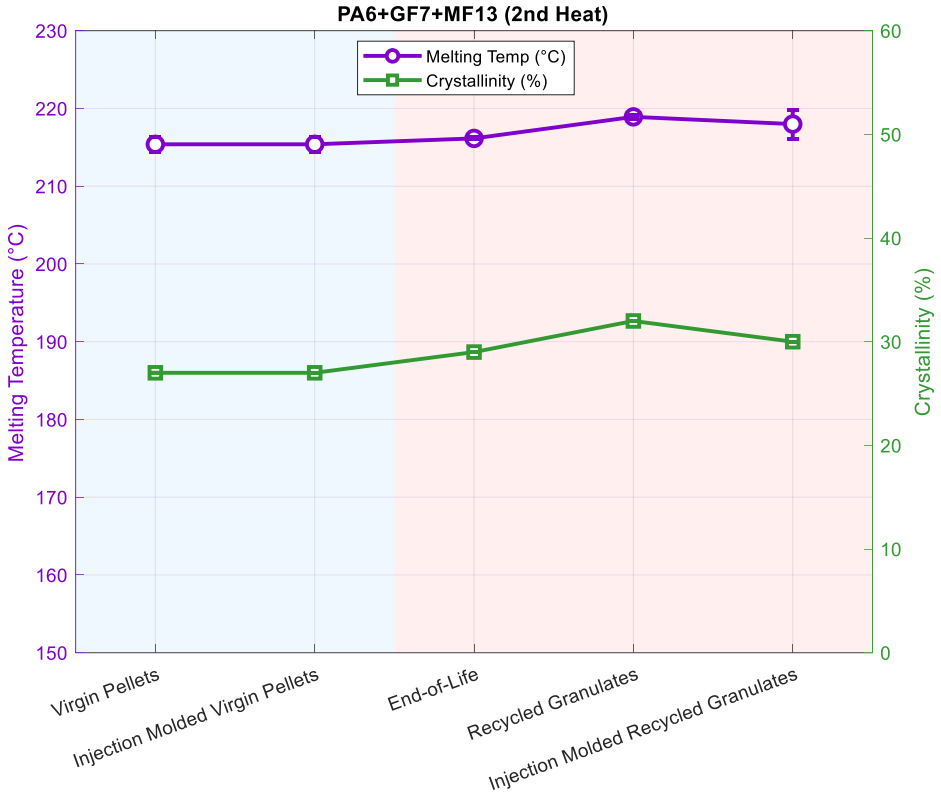


Figure 5.7 - Melting temperature and crystallinity for PA6+GF7+MF13 samples across all .processing stages, based on second heat thermal analysis

VITA

Neeki Meshkat was born and raised in Nashville, Tennessee. From an early age, she developed a strong interest in STEM fields, particularly those connected to healthcare. This passion led her to pursue a bachelor's degree in biomedical engineering at the University of Tennessee, Knoxville. During her undergraduate studies, she became increasingly interested in the practical applications of engineering in medicine, which motivated her to continue her education through the university's five-year BS/MS program. She is currently completing her master's degree in mechanical engineering. Throughout her time at UT, she has remained focused on bridging engineering innovation with medical impact and plans to continue this work in the medical device industry after graduation.